


The Board of Trustees of the  
Leland Stanford Junior University  
Center for Materials Research  
Stanford, California 94305-4045  
Santa Clara, 12th Congressional District

Final Technical Report  
on  
**PROTEIN CRYSTAL GROWTH IN LOW GRAVITY**  
NASA #NAG8-774  
CMR-93-1  
SPO#7218  
for the period  
April 27, 1989 through December 31, 1992

Submitted to  
George C. Marshall Space Flight Center  
ES-76, Space Science Lab  
MSFC, AL 35812

Principal Investigator:

  
Robert S. Feigelson, Professor (Res.)  
Center for Materials Research  
Stanford, California 94305-4045  
(415) 723-4007

January 1993

## ABSTRACT

This Final Technical Report for NASA Grant NAG8-774 cover the period from April 27, 1989 through December 31, 1992. It covers five main topics: fluid flow studies, the influence of growth conditions on the morphology of isocitrate lyase crystals, control of nucleation, the growth of lysozyme by the temperature gradient method and graphoeptaxy of protein crystals. The section on fluid flow discusses the limits of detectability in the Schlieren imaging of fluid flows around protein crystals.

The isocitrate lyase study compares crystals grown terrestrially under a variety of conditions with those grown in space. The controlling factor governing the morphology of the crystals is the supersaturation. The lack of flow in the interface between the drop and the atmosphere in  $\mu g$  causes protein precipitation in the boundary layer and a lowering of the supersaturation in the drop. This lowered supersaturation leads to improved crystal morphology.

Preliminary experiments with lysozyme indicated that localized temperature gradients could be used to nucleate crystals in a controlled manner. An apparatus (Thermonucleator) was designed to study the controlled nucleation of protein crystals. This apparatus has been used to nucleate crystals of materials with both normal (ice-water, Rochelle salt and lysozyme) and retrograde (horse serum albumin and  $\alpha$  chymotrypsinogen A) solubility. These studies have lead to the design of an new apparatus that small and more compatible with use in  $\mu g$ .

Lysozyme crystals were grown by transporting nutrient from a source (lysozyme powder) to the crystal in a temperature gradient. The influence of path length and cross section on the growth rate was demonstrated. This technique can be combined with the Thermonucleator to control both nucleation and growth.

Graphoeptaxy utilizes a patterned substrate to orient growing crystals. In this study, silicon substrates with  $10\mu$  grooves were use to grow crystals of catalase, lysozyme and canavalin. In all cases, the crystals grew oriented to the substrate. The supersaturation needed for nucleation and growth was lower on the patterned substrates. In some cases, isolated, large crystals were grown.

## TABLE OF CONTENTS

<b>ABSTRACT</b>	<b>i</b>
<b>TABLE OF CONTENTS</b>	<b>ii</b>
<b>I. INTRODUCTION</b>	<b>1</b>
<b>II. RESEARCH RESULTS</b>	<b>2</b>
A. FLUID FLOW STUDIES	2
B. INFLUENCE OF GROWTH CONDITIONS ON THE MORPHOLOGY OF ISOCITRATE LYASE CRYSTALS	3
C. CONTROL OF NUCLEATION	8
D. GROWTH OF LYSOZYME BY TEMPERATURE GRADIENT ( $\Delta T$ )	14
E. GRAPHOEPI TAXY	17
<b>III. REFERENCES</b>	<b>24</b>
<b>IV. PUBLISHED PAPERS</b>	<b>26</b>
<b>V. FIGURES</b>	<b>27</b>

## I. INTRODUCTION

The research reported on in this final report had as its objective the study of the effect of low gravity on the growth of protein crystals and those parameters which will affect growth and crystal quality. The proper design of the flight hardware and experimental protocols are highly dependent on understanding the factors which influence the nucleation and growth of crystals of biological macromolecules. Thus, the primary objective of this research was centered on investigating those factors and relating them to the body of knowledge which has been built up for "small molecule" crystallization. This data also provides a basis of comparison for the results obtained from low-g experiments.

The main component of this research program was the study of mechanisms involved in protein crystallization and those parameters which influence the growth process and crystalline perfection. Both canavalin and lysozyme were used as the basic model proteins in these studies. Other biological macromolecules were included in this research program when they provide an opportunity to better understand the nature of the crystallization process. The program involves four broad areas:

1. The application of both classical and novel chemical and physical techniques to study the fundamentals of protein crystallization. Included in this area was a study of the phase relationships in the systems of interest, primarily the factors controlling solubility, the study of growth kinetics to determine the growth rate controlling mechanism and the relevant activation energy involved in the process. The effects of fluid flow on the growth and perfection of protein crystals were studied using flow visualization techniques.
2. Characterization of protein crystals. Optical microscopy gave a general evaluation of crystal morphology, size and perfection. Phase contrast techniques gave enhanced contrast to the surface features allowing observation down to the  $0.1\mu$  level.
3. Control of nucleation and growth. The information developed in the phase relationship studies of section 1) was used to design experiments to separately control the nucleation and growth processes. The information from section 2) was used to optimize the growth.
4. The design and construction of a prototype of space flight hardware. The design incorporated the results of section 3).

## II. RESEARCH RESULTS

### A. FLUID FLOW STUDIES

The analysis of the flows around growing crystals begun during the previous grant (NAG8-489) has been continued. In a previous report,<sup>[1]</sup> it was noted that flows had been observed around growing crystals of Rochelle salt, lysozyme and canavalin using the Schlieren imaging technique. The values for the change of density and index of refraction with change of concentration for each system were also reported. The change in density and index of refraction with concentration do not by themselves indicate whether flow will occur and, if it does, whether that flow can be imaged. The Grashof number,

$$Gr = \frac{g\Delta\rho}{\rho\nu^2} L^3$$

( $g$  is the acceleration of gravity,  $\Delta\rho$  the change in density across the diffusion boundary layer,  $L$  the characteristic length of the system-taken to be the height of the crystal,  $\rho$  the density and  $\nu$  the viscosity) is a non-dimensional, fluid dynamic variable that relates the buoyant force to the viscous drag. The larger this number, the more likely that flow will occur. More importantly, systems with the same Grashof number should behave alike. Thus, if a range of values of Grashof numbers can be established over which flow can be demonstrated to occur in crystallizing systems, then calculation of a Grashof number for a new system (macromolecular or not) will predict if flow should occur in that system.

Similarly, the ability to image the flow is not directly dependent on the change of index of refraction with concentration, but is related to the local change in light intensity

$$\Delta I/I = (f_2/a) \int (1/n) (\partial n/\partial x) dz$$

where  $f_2$  is the focal length of the second mirror in the Schlieren optics,  $a$  the knife edge aperture,  $n$  the index of refraction,  $\partial n/\partial x$  is given by  $(dn/dc)(\partial c/\partial x)$  where  $x$  is the direction across the plume, and  $dz$  is perpendicular to the plan of the film. Again it should be possible to establish a range of values under which the flows will be visible. Comparisons of new systems will establish the possibility of flow visualization.

In addition to the values for the changes in density and index with concentration, it is necessary to establish the actual concentration at the crystal interface. For a crystal growing under diffusion control (Rochelle salt), it is equal to the solubility. However, lysozyme<sup>[2]</sup> and canavalin<sup>[3]</sup> grow under interface control and the interface concentration may be estimated by using a method outlined by Pusey and Naumann.<sup>[4]</sup> Using these estimates, the Grashof number and the local change in light intensity for each system have now been calculated under

the experimental conditions. The values of the Grashof number are 772.48 for Rochelle salt, 23.04 for lysozyme and 67.84 for canavalin. If the Grashof number is normalized by fixing the size of the crystals at 1mm, then the Grashof numbers become 112.64 for Rochelle salt, 7.04 for lysozyme and 8.96 for canavalin. There is a much lower tendency for the protein solutions to experience convection under the conditions of these experiments even when size considerations are taken into account, but flow does occur in all these systems. The values found for the local change in intensity are 21.7 for Rochelle salt, 2.93 for lysozyme and 4.39 for canavalin. Based on the image quality of the films used in this study, the value of 2.39 appears to be near the limit of detectability in our system (400ASA film, f2.8, 1/51 sec exposure).

#### **B. INFLUENCE OF GROWTH CONDITIONS ON THE MORPHOLOGY OF ISOCITRATE LYASE CRYSTALS**

The structure of the protein isocitrate lyase (ICL) has been under study for a number of years at Du Pont Merck. Attempts to grow isocitrate lyase crystals by the hanging drop method produced crystals with very poor growth morphologies (Fig. 1). It was not immediately clear whether this poor morphology was due to unstable growth conditions or sedimentation. A series of experiments were designed to answer this question. In addition to the ground based experiments, ICL has been flown as part of the NASA shuttle program. As a result of these experiments and the application of theoretical evaporation models to the crystallizing system, factors affecting the growth of ICL crystals and, by extension, other protein crystals became apparent.

All of the ICL used in these experiments came from Du Pont Merck. Before use, the ICL solution (ICL in 0.1M Tris-HCl pH 7.8, 10mM EDTA, 1mM DTT, 0.4M KCl) was incubated at 4°C for 24 hrs with a reducing solution (0.3M Glutathione, 66mM EDTA in 1M Tris-HCl pH 8.0) (4:100 v/v) and an inhibitor solution (50mM 3-nitropropionate, 0.5M MgOAc in 50mM Tris-HCl pH 7.0) (4:100 v/v). The ICL concentrations were 10mg/ml (Du Pont Merck) and 12mg/ml (Stanford). The well solution was 1.6-2.0M (60-80% saturation) Na-citrate (Na-cit). The usual drop size was 4 $\mu$ l (2 $\mu$ l ICL solution and 2 $\mu$ l well solution). Crystals appeared within one week at 24°C.

The source of the poor morphology was investigated by closely observing drops during crystallization. These 4 $\mu$ l hanging drops (12mg/ml ICL solution, 72% Na-Cit well solution) were observed through a microscope at 150x.

Figure 2 shows a typical result of the 4 $\mu$ l hanging drop experiments. The crystal is more obviously dendritic than those grown from a 30 $\mu$ l drop (Fig. 1). It is obvious that the poor morphology resulted from uncontrolled growth originating at the corners of the crystal.

Such growth can result from either excessive supersaturation<sup>[5]</sup> or from flow effects.<sup>[6]</sup> In an attempt to separate these effects, a glass Schlieren imaging cell (1mm x 3mm rectangular cross-section) was built and 4μl of ICL crystallizing solution was vapor equilibrated against Na-cit in the well of the cell. While no flows were observed, in this experiment, the three crystals were found growing in this cell had a more regular morphology than had been previously observed in the hanging drop experiments (Fig. 3).

The same growth experiment was repeated in circular cross section capillaries (1.88mm diameter) to better observe the crystals. The ICL crystals grown in these capillaries exhibited a very well formed morphology (Fig. 4). These crystals have been x-rayed and have the same space group (P2<sub>1</sub>2<sub>1</sub>2<sub>1</sub>) and unit cell parameters (a=80.7Å, b=123.1Å, c=183.4Å) as the previously grown crystals. The "octagonal" cross-section arises from the orthorhombic symmetry with the facets bounded by (100), (010) and (110) faces. The end of the crystals are bounded by either (001) (flat) or (101) (wedge shaped) faces.

A comparison of Figs. 2 & 4 shows that the initial breakdown in morphology occurs at the corners of the crystal. This breakdown is probably associated with excessive supersaturation and, thus, with unstable growth conditions.

Sibille and his co-workers have developed mathematical models to describe the evaporation from both drops and capillaries in equilibrium with well solutions.<sup>[7,8]</sup> These models may be expressed in the general form as:

a) for the hanging drop

$$t / t = F[x(t)]$$

and b) for the capillary

$$t / t = G[\partial(t)]$$

where

$$x(t) = \frac{a(t)}{a_0}; V(t) = \Omega_v(\alpha) a(t)^3; \Omega_v(\alpha) = \frac{4}{3} \pi \cos^4\left(\frac{1}{2} \alpha\right) [1 + 2 \sin^2\left(\frac{1}{2} \alpha\right)]$$

where  $\alpha$  is the contact angle of the drop, and

$$\partial(t) = \frac{\Delta_1(t)}{\Delta_1(0)}; \Delta_1(t) = n_1(e)[t] - n_1(c)[t]$$

where  $n_1(e)[t]$  is the number of moles of water in the crystallizing solution and  $n_1(c)[t]$  the number of moles of water in the well. The characteristic times,  $t$ , for the two models are defined by:

a) for the hanging drop

$$\tau = \frac{3 \Omega_v(\alpha) a_0^2 n_1(b) R T}{\Omega_a(\alpha) D_1 p_1^0 w n_2(b) V_1}; \Omega_a(\alpha) = 4 \pi \cos^2\left(\frac{1}{2} \alpha\right)$$

and b) for the capillary

$$\tau = \frac{R T L \Delta_1^2(0)}{4 S D_1 p_1^0 w n_2}$$

where  $n_1(b)$  is the number of moles of water in the well,  $D_1$  the diffusion coefficient of water in air,  $p_1^0$  the vapor pressure of pure water,  $w$  the vapor pressure lowering constant,  $n_2(b)$  the number of moles of precipitant in the well,  $V_l$  the partial molar volume of water,  $L$  the distance between the crystallizing solution and the well,  $S$  the cross sectional area of the capillary,  $n_2$  the total number of moles of precipitant in the crystallizing solution and the well, and  $R$  and  $T$  have their usual meaning. The parameters needed to use these models for ICL and lysozyme were calculated as outlined in ref. [7] The osmotic coefficient for Na-cit was estimated using equation 10, section 14 of Shoemaker and Garland.[9] The contact angle for the hanging drop simulations was  $90^\circ$ , the well volume  $500\mu\text{l}$  and the spacing  $5\text{mm}$ . The well volume for the capillary simulations was  $350\mu\text{l}$  and the spacing was  $3.5\text{cm}$ . Figure 5 compares the results of applying these models to a drop and a  $1.88\text{mm}$  ID capillary containing the same volume of ICL solution. The drop evaporates at a rate which is two orders of magnitude faster than the capillary. This difference in rates is consistent with laboratory observations.

The rate of change of supersaturation is somewhat more complicated than the rate of change in volume of the crystallizing solution since the concentration of both the crystallizing species and the precipitant change with the change in volume and, through the solubility curve, both affect the supersaturation. The supersaturation is further affected by the growth of crystals in the solution. Unfortunately, neither the solubility curve nor the growth kinetics of ICL is known. In order to estimate how supersaturation would change during crystal growth by vapor equilibration, the models of Sibille et al.[7,8] were applied to lysozyme crystallization using the solubility data reported by Pusey[10] and the growth kinetics described by Pusey and Naumann.[4] The growth solution modeled contained  $30\text{mg/ml}$  lysozyme and  $2\%$  NaCl equilibrated against a well of  $4\%$  NaCl. Ten crystals were assumed to nucleate at  $c/s = 4$  (a value consistent with other studies). No further nucleation was allowed to take place. The amount of lysozyme removed from solution during each growth period was determined. Figure 6 shows the results for both a hanging drop and a capillary. The supersaturation in the drop reaches a peak which is almost double that of the capillary. The crystallizing system can react to this increased supersaturation by either 1) nucleating more crystals (secondary nucleation), 2) increasing the growth rate to the point of instability, or 3) a combination of the two. Lysozyme does the latter exhibiting secondary nucleation together with surface roughening. ICL, on the other hand, exhibits morphological instability.

Figure 7 shows an ICL crystal which was grown by Du Pont Merck in low-g during a shuttle mission. The morphology is greatly improved over those grown by the hanging drop technique on Earth. The drops used in space were larger ( $30\mu\text{l}$  vs.  $4\mu\text{l}$ ) than those used on



Earth which raises the question of whether the improvements in crystal quality are related to the effects of  $\mu\text{g}$  or simply the difference in evaporation rate. Figure 8 shows the theoretical evaporation rates for  $4\mu\text{l}$  and  $30\mu\text{l}$  drops. The rate of equilibration was 5x slower for the larger drop, but the crystals shown in Figs. 1 & 2 were grown under the same conditions. While there was some improvement in the morphology of the 1-g crystal grown from a  $30\mu\text{l}$  drop (Fig. 1), the decrease in equilibration rate can not satisfactorily explain the greatly improved morphology found in the ICL crystals grown in space from the same size drop.

There are other factors which may affect the morphology of space grown crystals. It has been pointed out<sup>[7]</sup> that drops evaporate slower than predicted in space due to the existence of a concentrated layer of precipitant near their surfaces which lowers the vapor pressure of the drop and retards evaporation. The preliminary data in ref. [7] indicated that the rate of evaporation decreased by a factor of about 2. This would produce a lower evaporation rate (10x) for  $30\mu\text{l}$  drops in  $\mu\text{g}$  compared to  $4\mu\text{l}$  drops at 1-g. This is still an order of magnitude faster than the equilibration rates for the capillary experiments. Clearly, the reduced equilibration rate due to the presence of a concentrated salt layer at the liquid-vapor interface was not the only factor contributing to the improved quality of the space grown ICL crystals.

In an attempt to simulate  $\mu\text{g}$  conditions on the ground and to provide a further basis for comparison between protein crystal growth at 1-g and  $\mu\text{g}$ , a series of capillary ICL crystal growth experiments were performed together with some simulated growth experiments (identical solutions without protein). Experiments were conducted with the capillary in both the normal and inverted positions. In the latter case, it was hoped that gravity would stabilize the denser salt layer at the liquid-vapor interface. In the simulated growth experiments, the inverted capillaries equilibrated at a slightly slower rate. In the actual growth experiments, a precipitate layer appeared at the liquid-vapor interface in the inverted capillaries. No precipitate was found in the normal capillaries, nor did such layers appear in the simulated growth experiments and it must be concluded that the precipitate was isocitrate lyase. In some cases crystals eventually grew in this layer. The existence of the precipitate in the surface layer decrease the supersaturation in the ICL solution in the same manner as the growing crystals did in the lysozyme growth simulation. Therefore, the ICL crystals were actually growing from a lower supersaturation than would be expected on the basis of evaporation alone. If Sibille's model of the stable surface layer in  $\mu\text{g}$ <sup>[7]</sup> is correct, then this mechanism can explain the improved crystal morphology seen in the ICL  $\mu\text{g}$  experiments.

"Octagonal" ICL crystals were only observed in the normal capillary configuration. This configuration promotes solutal convection. The solute Rayleigh number based on a ICL crystallizing solution with a depth of 7.2mm is approximately  $2 \times 10^6$  which is in excess of the critical Rayleigh number for aqueous solutions of 300. Even correcting for the size of the

capillary, the Rayleigh number would be as high as  $10^4$ . The time for onset of convection calculated from the time dependent Rayleigh number was approximately  $1 \times 10^{-3}$  seconds. There will be mixing in this configuration and the results indicate that some degree of mixing is desirable in the growth of ICL from capillaries.

The poor morphology of the ICL crystals grown by the hanging drop method in 1-g was due to high (unstable) growth rates due to high supersaturation. While it is necessary in all unseeded "batch" type crystal growth to increase the supersaturation high enough to cause nucleation, a slower rate of increase of the supersaturation does lead to more controlled growth and crystals with better morphology. This effect is further mitigated by the presence of growing crystals or a precipitate both of which will act to lower the overall supersaturation. The slow rate of supersaturation can be achieved by using vapor diffusion equilibration in small diameter capillaries. An alternative approach which is potentially more controllable is to use the method proposed by Wilson and co-workers<sup>[11]</sup> in which flowing nitrogen of controlled humidity controls the rate of evaporation.

The ICL growth experiments conducted in the capillaries indicate that some convective mixing is beneficial to the crystal growth by providing mixing and a uniform supersaturation in the crystallizing solution. Pusey and co-workers<sup>[12]</sup> have demonstrated in the case of lysozyme that high flow rates can cause cessation of growth. However, most small molecule aqueous crystal growth is done with some form of stirring (see i.e. Buckley<sup>[13]</sup> and Chernov<sup>[5]</sup>). The best crystals will be expected to be found between the extremes of no flow (mixing) and rapid flows which can cause cessation of growth in protein systems.

The usual flows found in protein crystallization are due to solutal convection where gravity acts on density differences at the growth interface or at the vapor-liquid interface where evaporation is taking place. These flows can be non-uniform and unpredictable. The capillary experiments with ICL may have been fortuitous in that the size of the capillary and the volume of solution may have provided a Grashof number which yielded a suitable flow regime for growth. It is possible to engineer growth systems to give the proper Grashof number if the parameters of the system are known. However, the need to quantify the parameters can be bypassed by using gravity as a variable. To date this parameter has been explored only at the limits available: 1-g and  $\mu\text{g}$ . Experiments in an induced artificial gravity between the extremes are needed to study the effect of gravity and flow on the growth and morphology of protein crystals.

## Summary

While the lack of fluid flow in a  $\mu\text{g}$  environment is a factor in the improved quality of space grown ICL crystals. The results of this study indicate that lack of fluid flow around the crystal may not be as important a factor as the lack of mixing in the drop itself. This lack of mixing in the drop allows the protein to precipitate at the liquid-vapor interface thereby lowering the supersaturation at which the crystal grows. This lowered supersaturation leads to a slower growth rate which improves the crystal morphology. More study is needed both in 1-g and  $\mu\text{g}$  to determine if this mechanism is operative in other protein systems.

### C. CONTROL OF NUCLEATION

It is well known that crystal growth involves two separate processes; 1) nucleation of the species desired, and 2) the growth of these nuclei into macroscopic crystals of suitable size and quality for the intended application. Nucleation involves a phase transformation in which a solid surface of the phase desired is created within a nutrient phase. The crystal growth process, on the other hand, involves heat and mass transport, i.e. removing the latent heat evolved during the crystallization process and supplying nutrient to the growing crystal at an appropriate rate. It is not surprising, therefore, that the energetics involved in these two processes are not the same. In many cases, they are significantly different.

It is of practical importance to be able to isolate and control the nucleation process separately from the subsequent growth phase. In small molecule crystal growth, this is most often accomplished by introducing an appropriate seed crystal (usually of the material being grown) into a melt, vapor, or solution. The use of a seed by-passes the nucleation stage by providing the solid-liquid interface necessary for the crystal growth process to proceed. In the growth of crystals containing biological macromolecules, obtaining seeds of the appropriate size and quality is often very difficult and has rarely been an attractive strategy. In most macromolecular crystal growth processes currently in use, the nucleation step is achieved in the growth solution under poorly understood conditions and the growth proceeds in a more or less uncontrolled manner.

In crystal growth from aqueous solutions, (the principal, if not only method, for growing crystals of biological species) the driving force of nucleation is the supersaturation. The supersaturation,  $c/s$ , where  $c$  is the actual solution concentration and  $s$  is the concentration at the saturation point, provides the excess energy needed to form the solid surface in the solution phase (homogeneous nucleation). The temperature-composition diagram in Fig. 8 illustrates the relationship between solubility and supersaturation. The solid line is the solubility curve, which divides the diagram into two regions: unsaturated and supersaturated.

A second curve, the supersolubility curve, divides supersaturated region into labile and metastable regions. The labile region is unstable and nuclei form readily by spontaneous fluctuations in composition. Solutions are quite stable in the metastable state and it is only in this region where controlled crystal growth is possible.<sup>[5]</sup> The width of the metastable region depends on a number of factors, including purity of the starting materials. The supersaturation needed for homogeneous nucleation is often significantly greater than that needed for growth and that is why, after the initial nuclei are formed, growth normally proceeds in a rapid uncontrolled manner. The supersaturation necessary for nucleation can often be reduced if a foreign substance is present upon which the species of interest prefers to nucleate (heterogeneous nucleation).

Starting from an undersaturated condition, the metastable region can be reached in principle by either changing temperature at constant composition or composition at constant temperature. Most biological macromolecular crystals are grown by the latter technique because the temperature dependent coefficient of solubility (phase equilibria) is usually not known and, in some cases, is negligible. In Fig. 9, the phase diagram for canavalin is given showing regions of both temperature dependent and independent solubility.<sup>[14]</sup>

With respect to both nucleation and growth processes, temperature change methods are usually easier to control with more precision than other techniques such as evaporation and therefore, if possible, would be the method of choice.

One method for controlling nucleation without using seeds involves the localized control of supersaturation in a specific region of a near-saturated bulk solution. By doing so, nucleation will be confined to a small volume of the solution and the number of crystallites which form will thus be severely limited. With the bulk of the solution near or just at saturation, the crystals nucleated can then be grown in a controlled manner by changing the solution temperature and hence the bulk supersaturation.

### 1. Preliminary Controlled Nucleation Experiments

The solubility diagrams of both lysozyme<sup>[10]</sup> and canavalin<sup>[14]</sup> show a temperature dependence of the solubility. Based on this knowledge, preliminary controlled nucleation experiments using lysozyme have been conducted. These initial experiments used a small, temperature controlled spot to induce nucleation at a fixed position and to limit the number of nuclei produced. These experiments used lysozyme (20mg/ml, pH 4.0, 0.1M sodium acetate, and 4% sodium chloride). This solution will spontaneously nucleate in 4-5 days at room temperature. By using a cold spot temperature of 9°C, nucleation was accomplished in 5 hours. The number of nuclei was less when compared to the isothermal solutions, but they were not localized to the extent anticipated (Fig. 10).

## 2. Apparatus for Controlled Nucleation

The results of the preliminary localized nucleation experiments has led to the design and construction of the first prototype space flight hardware. This design incorporates a more sophisticated localized temperature gradient control as well as a means of controlling the ambient temperature around the growth cell as an aid to localizing the nucleation as well as a means of controlling subsequent growth. The apparatus (called the Thermonucleator) also has provisions for in situ microscopy, the inclusion of schlieren optics, and the optical detection of the onset of nucleation (Fig. 11). The actual apparatus is shown in Fig. 12.

The thermal environment in the cell was probed using a thermocouple mounted on a x-z positioner. With this device, temperatures could be measured across the cell at various heights above the bottom. A set of profiles taken with the temperature surrounding the cell set at 25°C and the cold spot set at 15°C is shown in Fig. 13. The resulting isotherms are plotted in Fig. 14. Two features should be noted in these figures (13 & 14). The bottom is warmer than the adjacent layer at 0.04mm at distances greater than 0.4cm from the cold spot. This is due to thermal convection in the volume above the cold spot and stagnation in these warmer regions. Second, the cold spot temperature is lower than the set temperature due to the position and type of thermocouple chosen for the control thermocouple. This will be changed in the near future. The measured vertical temperature gradient above the cold spot is about 200°C/cm.

## 3. Growth of Materials with Normal Solubility

The procedure for nucleating a desired crystal is generally as follows: 1) The bulk solution is set at a near saturation (Fig. 15a). Under these stable conditions, critical size nuclei should not form. 2)  $T_s$  is adjusted so that the supersaturation is large enough to cause nucleation on the exposed surface of the cold probe (Fig. 15b). The amount of undercooling should be such that the surface of the copper is at a temperature just inside the labile region described in Fig. 8. If the phase equilibria data (solubility) is not known, it is a rather simple matter to empirically find the appropriate temperature to cause nucleation to take place on the cold finger. 3) After solid forms on the tip,  $T_s$  (and sometimes  $T_e$ ) is raised to try and dissolve all but a few of the crystallites which may form initially. In practice, this is difficult to achieve because it is hard to see very small crystallites in the growth cell. Laser light scattering techniques, when developed and incorporated into the system, should provide more control of this process. 4) After dissolving back the initial crystallites,  $T_s$  is decreased to that of the bulk solution. 5) The temperature of both the bulk solution and the tip are slowly lowered to cause growth to take place on the existing seed or seeds (Fig. 15c).

In this study, we report on preliminary results using the thermonucleator to control the nucleation and growth of ice, Rochelle salt, and lysozyme.

The Rochelle salt solution was prepared by the method of Holden and Morrison.<sup>[15]</sup> The salt was dissolved in hot deionized water (1.3 gm/gm of water) and then cooled to 24°C so that the excess solute would precipitate, leaving a just saturated solution at that temperature. Using a hypodermic syringe fitted with a 0.22μ filler, 1-2 ml of the saturated solution was transferred to the growth cell.

For the lysozyme growth experiments, 74 mg of commercial material (Sigma) was dissolved in a 2 ml of buffer solution (0.1 M sodium acetate at pH 4.0) to give a concentration of 37 mg/ml. To this solution, 2% NaCl (20mg/ml) was added. The solution was then transferred to the growth cell as described above. The solubility data used to adjust  $T_s$  and  $T_e$  was from Pusey.<sup>[10]</sup>

A Gyr Time lapse video system was used to monitor and record the growth process and for extracting data on growth rates.

### Ice-Water System

In the ice crystallization experiments, the ambient temperature was set at 30°C and  $T_s$  at the nominal freezing point of water, 0°C. Figure 16 is a sequence of photographs showing the growth of an ice crystal directly on the cold finger surface as a function of time. Note that the shape of the crystal mimics the shape of the isotherms shown in Fig. 14. Unlike the growth of Rochelle salt and lysozyme, the ice crystallization experiments are an example of melt growth. The liquid-solid growth interface of course represents the freezing point isotherm. The last frame in Fig. 16 shows that the process is reversible.

### Rochelle Salt

While the ice-water system was used to study the temperature profiles and temperature control aspect of the thermonucleator apparatus, Rochelle salt was used as a model material to study the nucleation and growth characteristics in a typical aqueous solution growth situation. Figure 17 shows a sequence of photographs taken from a time lapse video monitor. The solution initially saturated at 24°C was kept at 24°C in the enclosure, while  $T_s$  was lowered to 16°C. The first frame shows a small single crystal growing directly on the copper and subsequent frames show the crystal growing. Between frames 2 & 3, and 3 & 4  $T_e$  was manually lowered by 2°C each, causing the crystal to grow larger, with  $T_s$  allowed to reach  $T_e$  prior to cooling. A secondary crystallite can be seen growing to the right of the original crystal. It is not clear whether this crystal was present initially or nucleated at a later time but the former possibility is more likely. By programming the temperature at a slow, uniform rate, the size and quality of the crystal should be improved significantly.

## Lysozyme

Lysozyme was used as a model system representative of the growth of biological macromolecules. The sequence of photographs shown in Fig. 18 represent the first attempt to nucleate a protein on the cold finger. Initially,  $T_e$  was set at 25°C and  $T_s$  at 15°C. Within approximately 4.5 hours, the first crystal of lysozyme could be observed. Three crystallites can clearly be seen, even in the first photograph. After about 8 hours,  $T_s$  was allowed to equal  $T_e$  and  $T_e$  was kept constant for another 15 hours. During this period, several additional crystallites developed which can clearly be seen in the frame shot at 8:12 a.m. At this point,  $T_e$  was lowered in 2°C steps twice during a 26 hours period. One can see that under the cooling rate regime used, a cluster of crystals developed. However, the cluster lies exactly on the surface of copper cold finger.

In the latest lysozyme crystallization, the same crystallizing solution was used. The bulk temperature ( $T_e$ ) was set at 22°C and the cold finger temperature ( $T_s$ ) at 12°C. After 6.5 hrs, crystals appeared on the cold finger (Fig. 19) and  $T_e$  and  $T_s$  were adjusted to 20°C. Observation after an additional growth period of 15.5 hrs showed that there was a polycrystalline mass on the cold finger. The temperatures were raised ( $T_s$  to 28°C and  $T_e$  to 26°C) to dissolve all but a few of the crystals. When only a few crystals remained (after 7.5 hrs), the temperatures were lowered to continue the growth ( $T_e$ =21°C,  $T_s$ =20°C). The temperatures were lowered 2°C increments over the next few days as growth continued. The final temperatures were  $T_e$  =18°C and  $T_s$  =16°C. During this growth sequence (Fig. 19), one large (270 $\mu$ ) crystal and several smaller crystals were formed on the cold finger. The change in crystal size with time is plotted in Fig. 20. In spite of the cooling, the growth rate decreased, as shown in Fig. 21.

### 4. Nucleation of Materials with Retrograde Solubility

In the case of materials exhibiting retrograde solubility, the nucleating probe would have to be kept warmer than the surrounding solution and therefore significant thermal convection would be expected. To determine whether strong convection would a) prevent nucleation, b) cause nuclei to form away from the probe, c) cause the nuclei which form on the probe to move away from the probe tip and/or d) effect nucleation density, two proteins which have retrograde solubility were studied: 1) horse serum albumin (HSA) (MW  $\approx$  60,000), and 2) bovine pancreas  $\alpha$ -chymotrypsinogen A (aCA) (MW  $\approx$  26,000). In addition, these two proteins have another characteristic in common, while they are known to have retrograde solubility,<sup>[16,10]</sup> their actual solubility-temperature relationships in solution are not well characterized. The latter provided an excellent opportunity to study the ability of the

Thermonucleator to produce, within a short period of time, controlled crystallization in the absence of phase equilibria information.

The general approach used to nucleate these proteins without the benefit of knowing their solubility behavior was to prepare a near saturated to slightly supersaturated solution based on the known crystallization procedures<sup>[17,18]</sup> and to slowly raise the probe temperature until nucleation occurred. The ambient temperature was also increased to raise the saturation of the bulk of the solution.

The horse serum albumin (HSA) solution used for our nucleation study was based on the vapor equilibration crystallization outlined by McPherson.<sup>[17]</sup> In this work, the HSA solution (10mg/ml) was equilibrated against 45% saturated ammonium sulfate (0.31gm/ml) solution at room temperature. The HSA solution consisted of 10mg/ml HSA dissolved in water with 0.28mg/ml of ammonium sulfate added to produce a small amount of supersaturation.

The  $\alpha$ -chymotrypsinogen A (aCA) solution was the same as that used in the study by Matthews.<sup>[18]</sup> The retrograde solubility was tested by comparing two solutions: one at 4°C and the other at room temperature. The room temperature solution crystallized, but the 4°C solution did not. The aCA solution was made up by dissolving 16mg/ml of aCA in a buffer solution. The buffer solution contained 4% (v/v) ethanol and was 0.142M in dibasic potassium phosphate and 0.129M in citric acid. The precipitant was 60% by volume of a saturated ammonium sulfate solution.

The selected "retrograde" proteins (HSA and aCA) were successfully nucleated using the Thermonucleation technique (Figs. 22 & 23). The horse serum albumin crystals were nucleated on the probe at a temperature of 29°C, with the ambient temperature set at 16°C. The HSA crystal in Fig. 22 was approximately 20 $\mu$  at the widest point and was the largest crystal of this material observed in this series of experiments. The  $\alpha$ -chymotrypsinogen A crystals were nucleated at a probe temperature of 20°C with the ambient temperature set at 9°C. Figure 23a shows three aCA crystals at an early stage of growth (the largest crystal is about 27 $\mu$  along the base line). After a week of growth (Fig. 23b), the largest crystal is approximately 52 $\mu$ .

The actual nucleation and growth conditions for these crystals were not optimized, but represented a best estimate of the conditions based on the other growth techniques.<sup>[17,18]</sup> These results clearly demonstrated that the Thermonucleation technique can be applied to proteins whose solubility decreases with increasing temperature and to systems whose solubility behavior is known only in a general way (i.e., more crystals are formed if the temperature is lowered {raised}).

It has been suggested that the Thermonucleation technique could only be applied to solutions that were "sufficiently viscous to suppress convection to the extent necessary to



prevent nucleation in undesired sites." [19] The tendency of a solution to convect due to a temperature difference is given by the thermal Rayleigh number (Ra)

$$Ra = \frac{g c_p \rho^2 \beta L^3 \Delta T}{\mu k} \quad 1)$$

where  $g$  is the acceleration due to gravity,  $c_p$  the specific heat,  $\rho$  the density,  $\beta$  the thermal expansion coefficient,  $L$  the length (2cm),  $\Delta T$  the temperature difference (13°C),  $\mu$  the viscosity and  $k$  the thermal conductivity. Using equation 1 and the values for the material properties at 20°C, [20] Ra was calculated to be  $1.45 \times 10^6$ , which is well in excess of the critical Rayleigh number for the occurrence of natural fluid convection in these water solutions ( $\approx 300$  [21]). Strong flows were indeed observed by the movement of small particles in the growth cell. However, the results of the nucleation experiments indicated that crystals can be nucleated even in the presence of these flows.

## 5. Summary

An apparatus has for the first time been designed and built to control supersaturation in a localized region of a bulk solution, thereby permitting a separation of the nucleation and growth processes. The effectiveness of this "thermonucleating" device has been demonstrated with the nucleation and growth of materials with normal solubility such as ice, Rochelle salt, and lysozyme and also of materials with retrograde solubility such as horse serum albumin and  $\alpha$  chymotrypsinogen A. The method relies on the species to be grown having a temperature dependent solubility which may or may not be well known, but an alternative procedure could be devised to create the localized supersaturation by controlling composition in a small region of the solution. A more precise means of detecting nucleation must be developed to work in conjunction with localized supersaturation control.

## 6. New Apparatus

The current apparatus has been a useful tool for the development of the thermonucleation technique and will continue to be used to develop nucleation detection techniques. However, the size of the apparatus and its reliance on liquid nitrogen as a cooling source is not compatible with the use of the thermonucleator in  $\mu$ g. A new apparatus has been designed that uses thermoelectric elements for heating and cooling. Figure 24 shows the new apparatus which has dimensions of 4 x 3 x 3 inches and is designed to be plugged into a rack which would provide electrical connections, coolant and lighting for observation. Figure 25 shows the internal construction with the ambient temperature control elements sandwiched between the coolant plates and the plates which form the top and bottom of the temperature

controlled annulus. Control of the nucleation probe is provided by a similar sandwich assembly using one large thermoelectric element. The new Thermonucleator is currently under construction.

#### D. GROWTH OF LYSOZYME BY TEMPERATURE GRADIENT ( $\Delta T$ )

If a crystallizing material has a solubility which is dependent on temperature, then crystals can be grown by the transport of the material due to a temperature gradient. If Raoult's law is applied to solutions, the ratio of the solubilities ( $s/s'$ ) at any two temperatures ( $T, T'$ ) is given by

$$\ln (s/s') = \frac{\Delta H_f}{R} \left( \frac{1}{T'} - \frac{1}{T} \right) \quad 2)$$

where  $\Delta H_f$  is the heat of fusion of the solute and  $R$  the gas constant.<sup>[22]</sup> In the temperature gradient growth technique, the two solubilities occur in the same closed system which, in the absence of any convection, causes the diffusion of the soluble material from the high solubility region to the low solubility region due to the difference in chemical potential. This process is summarized for the normal solubility case in Fig. 26 which illustrates the use of a solubility curve and a temperature gradient to predict the movement of material from a source (at  $x+\Delta x$ ,  $T+\Delta T$  and solubility  $c+\Delta c$ ) to a growing crystal (at  $x, T$  and solubility  $c$ ). This technique is also applicable to systems with retrograde solubility, but the mass transport will be from  $T_{\text{cold}}$  to  $T_{\text{hot}}$ . The design of a crystallizer based on the temperature gradient technique and its application to the growth of the protein lysozyme will be discussed.

Lysozyme below 30°C exhibits a normal solubility vs. temperature behavior<sup>[12]</sup> and was chosen to test the feasibility of growing protein crystals by the temperature gradient method. The cell designed for this experiment is shown in Fig. 27. It consists of two microscope slides separated by a 0.0625 in spacer. The end temperatures were maintained by circulating water from temperature controlled baths through the ends. A uniform gradient was assured by the copper plate under the cell. The temperature gradient used and the resulting solubility profile are shown in Fig. 28. Figure 29 is the size of the crystal vs. time. The initial growth rate was 0.56 $\mu$ /hr which was about 10% higher than was predicted by Pusey and Naumann's data<sup>[4]</sup> when the high and low temperature solubilities were used to calculate the supersaturation. The growth rate drops to less than half the initial value (0.24 $\mu$ /hr) when the crystal reaches about 1050 $\mu$  in size. The reason for this behavior is unclear and it may be related to the "terminal size effect".

Figure 30 shows the resultant crystal photographed in transmitted light with crossed polarizers. The initial seed crystal appears a light rectangle within the crystal. The pictures show both the extensive secondary nucleation which took place and the surface structure which developed on the growing crystal.

One possible explanation for the secondary nucleation seen in Fig. 30 was that small particles of lysozyme were drifting down from the source material and growing in the cooled regions. In order to prevent this, the cell was modified with baffles as shown in Fig. 31, which also shows the positions of the growing crystals. The temperature gradient and solubility profile of this cell was slightly different (Fig. 32). The growth behavior of two of the crystals is plotted in Fig. 33. They exhibit different growth rates ( $0.35\mu/\text{hr}$  and  $0.27\mu/\text{hr}$ ) and both of these rate are below that which would be predicted ( $0.44\mu/\text{hr}$ ). One explanation for this is that in the first case the crystal was growing under the control of interface kinetics and in the second case there is mixed interface and diffusion control.

Figure 34 shows two of the crystal grown in the baffled cell. It is obvious that the baffles have not solved the problem of secondary nucleation.

Brice<sup>[23]</sup> has developed a general equation for the growth rate ( $f$ ) in the temperature gradient method which includes both the kinetic and transport processes

$$f \left[ \frac{\delta_c}{V_m D} + \frac{A_c \delta_n}{D A_n V_m} \right] + (f/A)^{1/n} = \sigma_e \frac{\Delta H \Delta T}{R T_e^2} \quad 3)$$

where  $\delta_{c,n}$  are the diffusion boundary layer thicknesses at the crystal and the nutrient ( $0.005\text{cm}$  <sup>[4]</sup>),  $A_{c,n}$  the areas of the crystal and the nutrient,  $A$  the kinetic coefficient ( $1.11 \times 10^{-9}\text{cm/sec}$  <sup>[4]</sup>),  $\sigma_e$  the supersaturation at the growth interface ( $C_e/C_s - 1$ ) ( $C_s = 14.3\text{mg/ml}$  <sup>[24]</sup>),  $\Delta H$  the heat of solution,  $\Delta T$  the temperature difference ( $9^\circ$ ),  $V_m$  the molar volume of the solute,  $D$  the diffusion coefficient ( $1 \times 10^{-6}\text{cm}^2/\text{sec}$  <sup>[4]</sup>),  $R$  the gas constant and  $T_e$  the temperature at the growth interface ( $16^\circ\text{C}$ ). The area of the crystal after 500 hrs of growth was  $0.05\text{cm}^2$  and the area of the nutrient was  $0.2\text{cm}^2$ . The heat of solution calculated from Raoult's law using the solubilities of lysozyme <sup>[24]</sup> at  $16^\circ\text{C}$  and  $25^\circ\text{C}$  was  $23,307\text{cal/mole}$ . The molar volume of lysozyme in solution calculated from the solution densities using equation 16, chapter VI of Shoemaker and Garland<sup>[25]</sup> was  $18,934\text{cm}^3$ . Using these values and the measured growth rate, the equilibrium concentration ( $C_e$ ) was calculated to be  $37.0\text{mg/ml}$ .

The preliminary study on the suitability of the temperature gradient method to the crystal growth of biological materials has demonstrated that this technique can be used for these materials. The results of this investigation pointed out the importance of the path dimensions

on the rate limiting step for the growth process. Future cells can be designed to maintain growth in the kinetically controlled regime.

As illustrated in Fig. 35, the analysis of the growth in a temperature gradient involves a large number of variables. The parameters effecting the solubility of the protein such as salt concentration, pH and buffers have not been included in this list but will be studied with the other parameters.

While the Thermonucleator can control the nucleation phase of the growth process, the size of the crystal that can be grown in the apparatus is limited by the volume of the solution, the concentration of the protein and the efficiency of crystallizing the protein from solution. The combination of the Thermonucleator with the temperature gradient technique would give the possibility of growing much larger protein crystals under well controlled conditions. This combined technique can be applied both at 1-g and in a microgravity environment.

#### E. GRAPHOEPI TAXY

The widely used hanging (or sitting) drop vapor diffusion technique<sup>[26]</sup> for protein crystal growth is not completely satisfactory. The growth of any crystal from solution without seeding requires that a critical nucleus be formed which, in turn, requires that the critical supersaturation be exceeded.<sup>[27]</sup> This critical supersaturation is in excess of that which is necessary for well-controlled growth and it leads to two effects: multiple nucleation of many small crystals and/or rapid growth leading to poor quality crystals. In addition, gravity usually causes the crystals to settle in the drop, resulting in clusters of misoriented crystals which are unsuitable for structure determinations.

A preliminary study on the use of graphoeptaxy (artificial epitaxy) to grow oriented crystals of the proteins catalase, lysozyme and canavalin has been completed. Graphoeptaxy employs a substrate patterned on a micron scale to induce an orientation to the growing crystals. While the basic technique has been used for the growth of inorganic crystals consisting of small molecules,<sup>[28]</sup> this study is the first successful application of artificial epitaxy to the growth of protein crystals. The closest previous work is that of McPherson and Shlichta<sup>[29,30]</sup> in which protein crystals were grown on minerals.

The substrates for the growth of the protein crystals in this study were single-crystal (100) -, (111) - or (211) - silicon (Si) wafers. A striated microrelief (5 $\mu$ m+ 5 $\mu$ m period, 1-2 $\mu$ m depth grooves) was prepared on these substrates by anisotropic etching so that the grooves were bounded by closely-packed (111) - faces typical of diamond-like crystals. The striations had defined crystallographic directions: <110> and <100> on the (100) - substrates, <110> and <211> on the (111) - substrates, and <110> on the (211) - substrates. In addition, a regular two-dimensional array of hexagonal holes about 6 $\mu$ m across and 1 $\mu$ m in depth and

15 $\mu$ m center-to-center distances were created on the (111) - substrates. After the microrelief was made, some of the substrates were thermally oxidized so that they were coated by an amorphous SiO<sub>2</sub> layer 0.3 - 0.4 $\mu$ m in thickness. In a given experiment, both oxidized and non-oxidized substrates were used.

All crystallizations were carried out at room temperature by variations of the vapor diffusion method.[26] In the case of catalase and lysozyme, crystals were grown in a Petri-dish-based apparatus commonly used for protein crystallization.[26] Substrates were placed on a pedestal and a peripheral well was filled by a precipitant solution. In the case of canavalin, crystals were grown in a plastic box (Crystal Plate) produced by Flow Laboratories for the crystallization of proteins. The crystallizing solution for catalase was prepared from catalase *penicillium microfungus octale*, mol. weight 300,000 (300 kDa). A fine-crystalline catalase suspension prepared according to ref.[31] was centrifuged for 40 minutes at velocity 8,000 rpm and the precipitate was dissolved in 0.05M sodium acetate buffer solution, pH 5.2, containing 0.5M ammonium sulfate. The solution containing 10 to 20mg/ml of the catalase was centrifuged just before crystallization and 5 to 10 $\mu$ l droplets of the solution were pipetted onto the substrates. The precipitant solution was usually 1.4M ammonium sulfate. In some experiments, an initial precipitant solution contained only 0.8M ammonium sulfate and the concentration was gradually increased up to 1.4M by introducing the sulfate via a hole in the top cover of the crystallization chamber.

The crystallization solution for canavalin contained canavalin (30mg/ml) dissolved in a pH 9.2 (ammonium hydroxide) solution with 1% sodium chloride (NaCl) added. In some experiments, detergents such as n-octyl  $\beta$ -D-glucopyranoside ( $\beta$ -octylglucoside,  $\beta$ -OG) and sodium dodecyl sulfate (SDS) were used. Both were found to be effective in the sense that more small crystallites were formed. As a counter-solution, an acetic acid (HAc) solution with pH between 5 and 6 was used. It was found that, at pH = 4, crystallization was uncontrollable, leading to precipitates, while at pH = 7 no crystallization occurred in a reasonable length of time (1 week). Three configurations were used for crystallization: standing droplet, hanging droplet (on a glass substrate without microrelief), and a droplet "sandwiched" between the substrate and the cover glass plate. The sandwiched droplet was the most effective for the crystallization of canavalin. This configuration also gave some insights into the features inherent in crystallization of proteins by artificial epitaxy.

The crystallizing solution for lysozyme was made from a buffer solution containing 30mg/ml lysozyme, 0.1 M sodium acetate (pH 4) with an equal volume of a 8% NaCl solution added so that the final solution concentrations were 15 mg/ml lysozyme and 4% NaCl. As a counter-solution, NaCl solutions with concentrations of 8% or 14% were used. The 8%

solution did not give any results in a week's time, while with the 14% solution, the first crystals appeared (as was observed at 100 x) in a day.

In situ-optical microscopy at magnifications from 50 x to 100 x was used to observe the growing crystal. All crystals studied were transparent, which allowed the micro-relief to be seen through them and thus it was possible to make conclusions on orientation effects.

The most valuable results were of a morphological nature and consisted of a comparison of crystallite orientation (their principal elements such as edges, diagonals, etc.) with respect to the microrelief.

As was noted above, the catalase crystals were grown in droplets. In this case, wetting of the substrate by the solution was moderate so that the contact angles of the droplets had some value between 60° and 90°C. Accordingly, the density of the crystal deposition on the substrate was different for different areas under a given droplet, being higher at periphery, where supersaturation (as a result of evaporation of the solvent) is larger, and lower in the central part of the droplet. In both regions, the majority of crystals grew with their edges parallel to the substrate striations (Fig. 36). In addition to the edge-parallel-to-striations orientation, sometimes the diagonals of the crystals were parallel to the striations (Fig. 37). Once deposited, the catalase crystals remained immobile and continued to grow preferentially in width, but also in height and in depth.

Important information about growth of catalase crystals on substrates with micro-relief is obtained by the investigation of the morphology of the face of the crystals resting on the substrate (backside morphology). Figure 38 shows the backside morphology of a crystal which was first mechanically detached from the substrate and then overturned. The rib-type structure of the backside indicates that the crystal had grown into the micro-relief after it was attached to the substrate. A similar behavior was also observed for canavalin crystals (see below).

One of the results obtained in this study was on the effect of reliefs of different symmetry and/or different profiles on the orientation of the crystals. The ratio of the number of oriented-to-nonoriented crystals in a given droplet in a given area, can serve as a quantitative measure of this effect. Based on such a measurement, the best orientation of catalase crystals was achieved, first, with striated micro-reliefs as opposed to the hexagonal-type holes, and, secondly, with the striated reliefs on  $\langle 100 \rangle$  - striped (100) - substrates and on (211) - substrates ( $\langle 110 \rangle$  stripes), as opposed to other directions of striations. For example, with  $\langle 110 \rangle / (100)$  substrates, about 80% of crystals had their edges parallel to the striations. The advantage of the striated relief was evidently connected with the principle morphology of catalase crystals, namely with the existence of rather distinctive edges (the crystals are bounded

as a rule by simple rhombohedral faces with only two of six faces being visible, while the other four faces form very narrow stripes).

In respect to the orientation relationships, it must be noted that although hexagonal-shaped pits were not effective for oriented crystallization, sometimes catalase crystals were oriented with their edges parallel to rows of the hexagonal pits.

The orientation mechanism(s) will be discussed in more detail below in relation to the data on canavalin and lysozyme crystals.

Canavalin crystals were also oriented on substrates with micro-relief and again striated relief was most effective. This is to be expected since canavalin crystals have a rhombohedral shape with rather sharp edges (see Fig. 36)<sup>[3]</sup> under the growth conditions employed in this study.

Figure 39 demonstrates the effect of the micro-relief which orients many (although not all) of the crystals.

As was noted above, the crystals were obtained in a "sandwich" system where solution can move. At least three events are inherent in such a system: a) crystals formed can change their orientation and position during relatively short time intervals, b) the crystals can be overturned, c) the crystals are often removed from the substrate to surrounding areas of solution.

The first type of event involved both movement from nonoriented-to-oriented and from oriented-to-nonoriented positions (sometimes also from one nonoriented to another nonoriented one). The changes were most remarkable for relatively small crystals, especially for relatively thin ones. On the other hand, the smallest (of the visible) crystallites which fill a single groove were as a rule in oriented positions even though they sometimes moved. This indicated that it might be possible to ensure better orientation by initially growing more small crystals. To test this, detergents such as  $\beta$ -OG and SDS were added to the crystallization solutions and, in fact, were found to be effective. The crystals formed were in general smaller in size.

Another feature observed in the sandwich version was the overturning of crystals. The period of the striations on the backside of overturned crystals was exactly equal to the period (groove plus hill) of the micro-relief. This confirmed that the backside morphology was a result of the crystal growing into the substrate during the first stage of their formation. The overturned crystals had striations parallel to both their edges and their diagonal, as well as non-parallel to any distinctive direction. The first two cases (parallel to edges and to diagonal) once again illustrates the effect of the relief in orienting the crystallites.

Only some preliminary results on artificial epitaxy were obtained with lysozyme. As is seen in Fig. 40, these crystallites have some of their edges parallel to the substrate striations as a demonstrating deposition orientation.

It is possible to distinguish at least five different orientation mechanisms operative in artificial epitaxy. These mechanisms, which can operate both separately and simultaneously<sup>[28,32]</sup> include: a) orientation by means of topographic micro-relief ("macroscopic Kossel-Strankei mechanism"), b) orientation under action of capillary forces, c) orientation by periodic thermal relief (in directional solidification of a melt), d) orientation by symmetric anisotropic deformation (mainly for solid-state crystallization), and e) orientation by cooperative rotations of crystals.

In the case of protein crystallization from solution, mechanisms (a), (b) and (e) could be operative. However, under conditions typical for these experiments, mechanism (e) which operates mainly at the stage of coalescence of crystals should be excluded. Mechanisms (a) and (b) remain and our results, as described above, indicate that both of these mechanisms are active.

In the figures presented, the oriented crystals are confined by the stripes, which supports the topographic mechanism. At the same time, there are many indications (especially with canavalin) that capillary forces are active in the orientation of the crystals. Among these are the phenomena of the "mooring" of relatively small crystals with larger ones and the orientation of the smallest (visible) crystals with the relief. The latter fact is worth a more detailed discussion. It is difficult to imagine that all these small crystals have a width exactly equal to the width of the relief grooves. Most probably, the crystals have a width smaller than that of the grooves and they take a symmetric position in respect to the grooves' wall due to the capillary mechanism.<sup>[33]</sup> Thus, based on the experimental results, a combined orientation mechanism including both topographic and capillary effects is operative in this case.

The action of detergents has an effect on these processes. When the protein solution with the detergent was placed on a substrate as a droplet, far better wetting (in comparison with a "normal" solution without detergent) was observed. This "macroscopic" effect is evidently related to molecular interactions in the solution facilitating, first, the formation of a large number of small crystallites and, second, the mobility of the crystallites in the solution. The mechanisms of the effect remain unclear.

The issue of initial stages of protein crystallization is of principal importance. In general, the specifics of protein crystallization in comparison with the classic ("small-molecule") crystal growth was discussed by Feigelson.<sup>[34]</sup> It is clear that in view of the role of the medium (in particular of water molecules) in formation of protein crystals, nucleation here is a far more complicated process than that for usual (small-molecule) materials. Nevertheless, for proteins, similarly to small-molecule materials, it is possible to distinguish between homogeneous and heterogeneous nucleation. In particular in our experiments, we were able to note a role of foreign particles in nucleation (at least for lysozyme). We compared



three cases: when the crystallization solution was filtered (0.5  $\mu\text{m}$  filter), when it was centrifuged, and when no special pretreatment was done. At some relatively small supersaturations in the centrifuged and untreated solutions, the first observable crystals appeared in a day (100 x optical microscope) and there were a large number of crystals which were nonoriented. Under the same conditions, in the filtered solution, the first crystals appeared in a week. Growth was rather sluggish and many of the crystals were oriented in respect of the micro-relief. In general, it was noted that the relief was rather active in causing crystallization. In a droplet covered area, with and without relief, nucleation under the same conditions occurred far more readily on the relief. This means that the "artificial lattice" inherent in artificial epitaxy (graphoepitaxy) serves as a heterogeneous catalyst for nucleation. In this respect, some comments should be made on the results of McPherson and coworkers concerning the heteroepitaxial growth of proteins on single-crystalline (mineral) substrates.<sup>[29,30]</sup> The authors reported the oriented growth of lysozyme on apophyllite, noting the relationship of lattice parameters of the two materials as it is considered in classic heteroepitaxy. An alternative explanation of their results can be found in the principles of artificial epitaxy. Macroscopic (more than one-monolayer-height), oriented steps can be present on cleaved or natural faces of crystals such as the minerals used in McPherson's experiments. These steps can, in principle, orient depositing crystals, especially if the crystals are relatively large as in the case of protein crystallization.

Finally, it should be noted that our experiments on oxidized and non-oxidized Si substrates have shown no difference in results, indicating that no orienting effects from single-crystalline substrates ("classic heteroepitaxy") take place.

### Summary

The results of these preliminary studies show that in the case of catalase, lysozyme and canavalin graphoepitaxy does cause orientation of the growing crystals. In most cases, the orientation is such that an edge of the growing crystal is parallel to the relief. In a few instances, the orientation is along the face diagonal of the growing crystal. The amount of misorientation between individual macroscopically oriented crystals is not known, but it is probably small. A cluster of such macroscopically oriented crystals which had grown together could yield preliminary structural data.

The orientation of the growing crystals is the result of two mechanisms. The first mechanism is a morphological one in which the edge of the crystal attaches the wall of edge of the relief. Smaller crystals are oriented within the relief by capillary forces. Both mechanisms may be active during growth.

There is evidence to suggest that the patterned substrates induce nucleation at lower supersaturation than would be necessary without the substrate. This is advantageous because, as was previously mentioned, it limits the number of nuclei and provides a slower growth rate which can lead to better crystals. In some cases (Fig. 39), large (100 to 200  $\mu$ ) crystals grow in isolation. These crystals can be used as seeds in one of two ways. If the space around the crystal is large enough, more nutrient solution can be added and the crystal grown out to a size suitable for diffraction studies. If there is not enough space to allow additional growth, the substrate can be cleaned of extraneous crystals and the seed grown to the desired size. The presence of the substrate facilitates the handling of the seed crystals.

### III. REFERENCES

1. Final Report, "Protein Crystal Growth in Low Gravity," NASA Grant NAG 8-489.
2. S. Durbin, Proc. of Third Int'l Conf. on the Crystallization of Biological Macromolecules, 13-19 August, 1989, Washington, D.C.
3. R. DeMattei and R. Feigelson, *J. Crystal Growth* **76**, 333 (1989).
4. M. Pusey and R. Naumann, *J. Crystal Growth* **76**, 593 (1986).
5. A. A. Chernov, Modern Crystallography III, Springer-Verlag, Berlin, 1984.
6. R.-F. Xiao, J. I. D. Alexander and F. Rosenberger, private communication.
7. L. Sibille and J. K. Baird, *J. Crystal Growth* **110**, 72 (1991).
8. L. Sibille, J. C. Clunie and J. K. Baird, *J. Crystal Growth* **110**, 80 (1991).
9. D. P. Shoemaker and C. W. Garland, Experiments in Physical Chemistry, McGraw-Hill, NY 1962.
10. E. Cacioppo, S. Munson, and M. L. Pusey, *J. Crystal Growth* **110**, 66 (1991); and E. Cacioppo and M. L. Pusey, in submission to *J. Crystal Growth*..
11. L. J. Wilson, T. L. Bray and F. L. Suddath, *J. Crystal Growth* **110**, 142 (1991).
12. M. Pusey, W. K. Withdrew and R. Naumann, *J. Crystal Growth* **90**, 105 (1988).
13. H. E. Buckley, Crystal Growth, John Wiley & Sons, NY 1951.
14. R. C. DeMattei and R. S. Feigelson, *J. Crystal Growth* **110**, 34-40 (1991).
15. A. Holden and P. Morrison, Crystal and Crystal Growing, The MIT Press, Cambridge, MA, 02142 (1982).
16. E. Cacioppo, private communication.
17. A. McPherson, Preparation and Analysis of Protein Crystals, (John Wiley & Sons, NY, 1982) ch. 4, p 128.
18. B. W. Matthews, *J. Mol. Biol.* **33**, 499 (1968).
19. NASA Tech Briefs **15**(9), 106 (1991).
20. B. Gebhart, Y. Jaluria, R. L. Mahajan, and B. Sammakia, Buoyancy Induced Flows and Transport, (Hemisphere Publishing Corp., NY, 1988) Appendix F, p 946.
21. G. Homsy, private communication.
22. F. T. Wall, Chemical Thermodynamics, (W. H. Freeman & Co., San Francisco, CA, 1958) ch.15, p. 322

23. J. C. Brice, The Growth of Crystals from Liquids, (North-Holland, Amsterdam, 1973) ch. 9, p. 297.
24. E. Cacioppo and M. L. Pusey, *J. Crystal Growth* 114, 286 (1991).
25. D. P. Shoemaker and C. W. Garland, Experiments in Physical Chemistry, (McGraw-Hill, NY, 1962) ch. VI, p 129.
26. A. McPherson, Preparation and Analysis of Protein Crystals, Wiley (1982).
27. H. A. Meirs and F. Issac, *Proc. Roy. Soc.* A79, 322, London (1907).
28. I. Givargizov, Oriented Crystallization on Amorphous Substrates, Plenum Press, NY (1990).
29. A. McPherson and P. Shlichta, *J. Crystal Growth* 85, 206 (1987).
30. A. McPherson and P. Shlichta, *J. Crystal Growth* 90, 44 (1988).
31. M. F. Gulyi, L. V. Gudkova, R. G. Deghtyar, N. I. Mironenko, and N. V. Latyshko, *Doklady of USSR Acad. Sci.* 225, 211 (in Russian) (1975).
32. E. I. Givargizov and A. B. Limanov, *Microelectronic Eng.* 8, 273 (1988).
33. V. I. Klykov and N. N. Sheftal, 52, 687 (1987).
34. R. S. Feigelson, *J. Crystal Growth* 90, 1 (1988).

#### IV. PUBLISHED PAPERS

1. R. C. DeMattei and R. S. Feigelson, "The Solubility Dependence of Canavalin on pH and Temperature," *J. Crystal Growth* 110, 34 (1991).
2. E. I. Givargizov, M. O. Kliya, V. R. Melik-Adamyan, A. I. Grebenko, R. C. DeMattei and R. S. Feigelson, "Artificial Epitaxy (Graphoepitaxy) of Proteins," *J. Crystal Growth* 112, 758 (1991).
3. R. C. DeMattei and R. S. Feigelson, "Controlling Nucleation in Protein Solutions," *J. Crystal Growth* 122, 21 (1992).
4. Robert C. DeMattei, Robert S. Feigelson and Patricia C. Weber, "Factors Affecting the Morphology of Isocitrate Lyase Crystals," *J. Crystal Growth* 122, 152 (1992).
5. R. C. DeMattei and R. S. Feigelson, "Thermal Methods in Protein Crystallization," Proc. 10th Int'l. Conf. on Crystal Growth, San Diego, CA, August, 1992.

## V. FIGURES

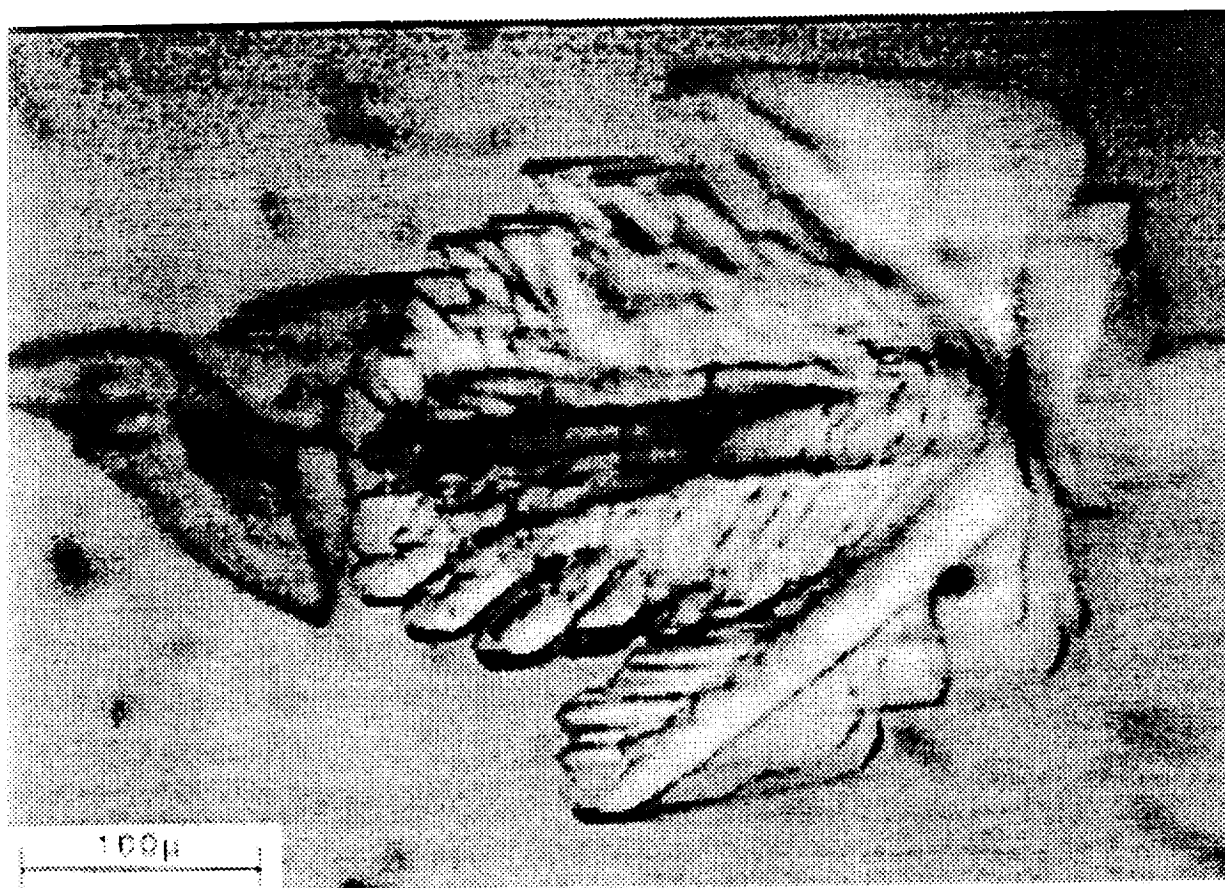


Fig. 1. Isocitrate lyase crystal (ICL) grown from 30 $\mu$ l hanging drop (ICL concentration 10mg/ml).

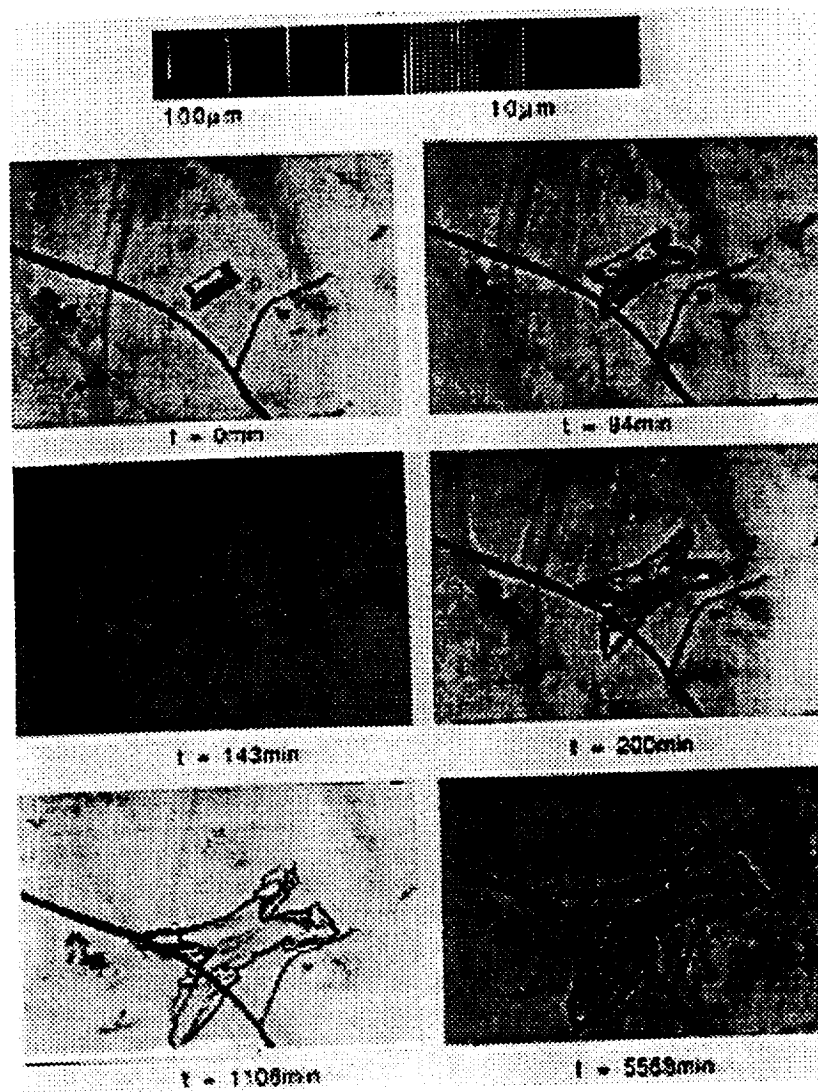


Fig. 2. Time lapse of ICL crystal grown from 4μl hanging drop (ICL concentration 12mg/ml).

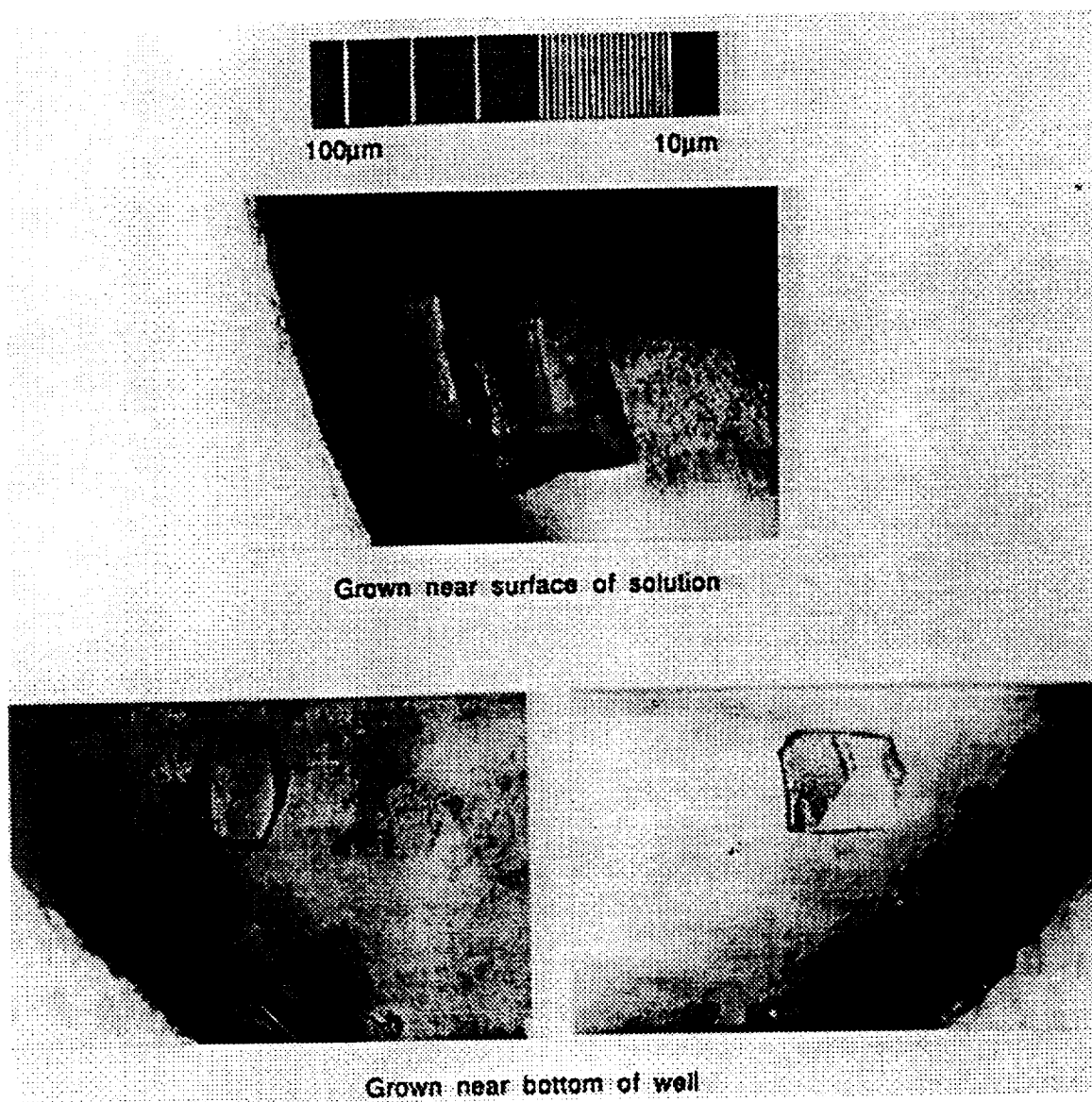


Fig. 3. ICL crystals grown in 1mm x 3mm cell (4μl of 12mg/ml).



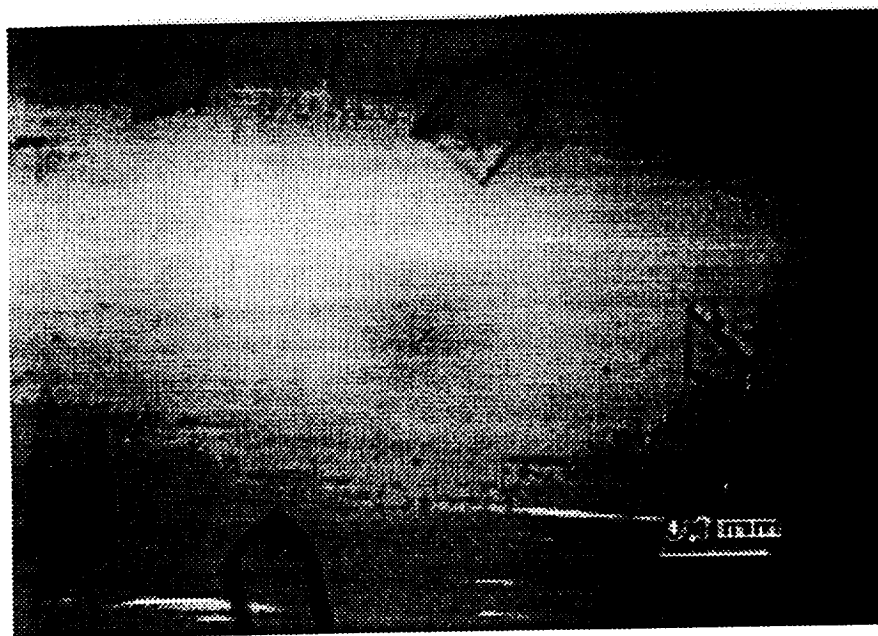
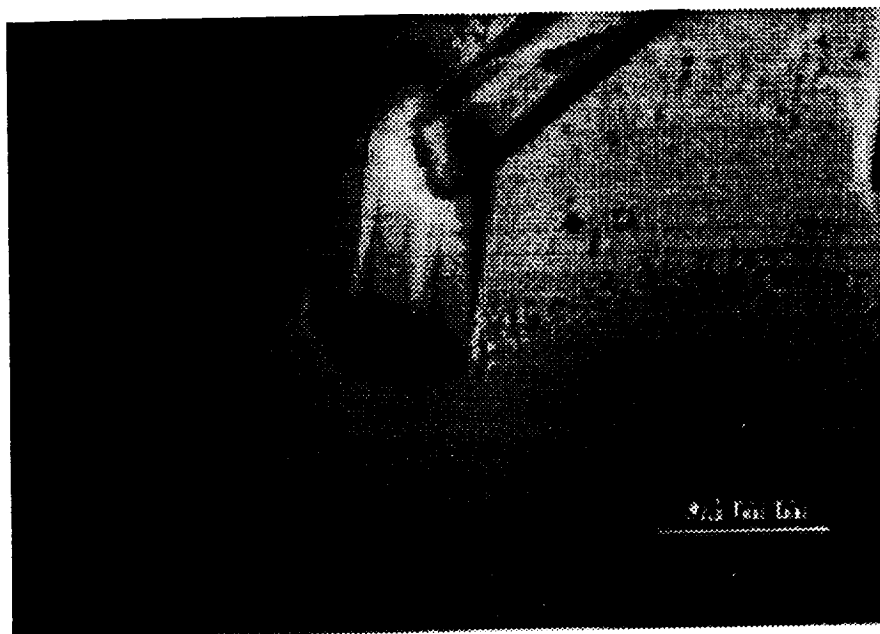


Fig. 4. ICL crystals grown in 1.88mm capillary (12mg/ml) showing a) flat termination by a (001) type face, and  
b) a wedged shaped termination by (101) type face.

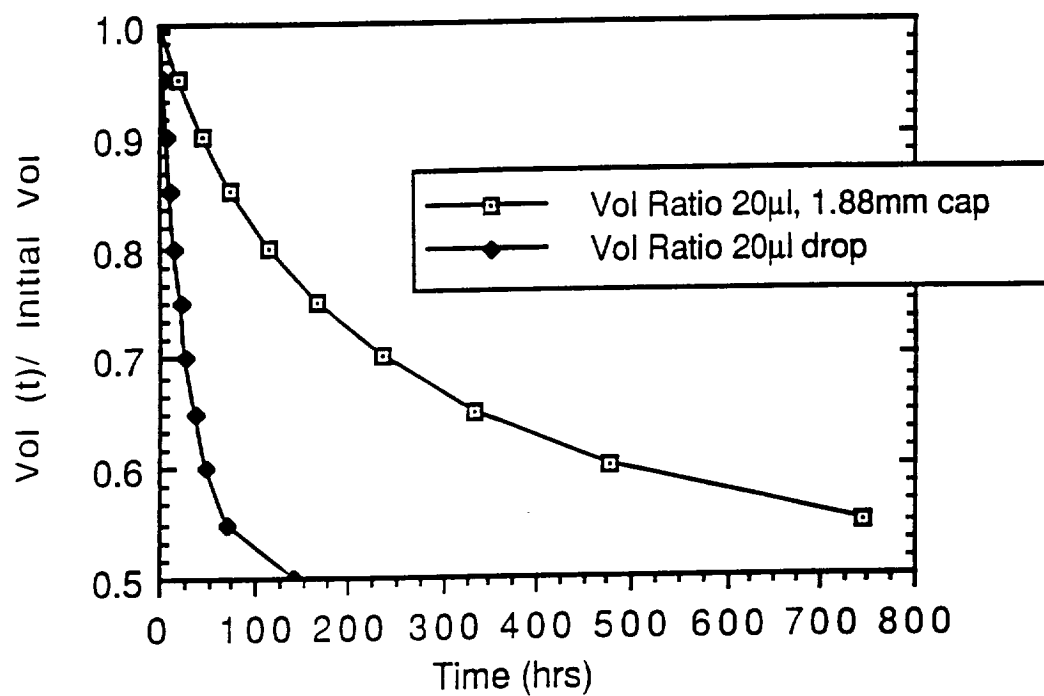


Fig. 5. Volume ratio vs. time comparing 20μl drop with 20μl in a 1.88mm capillary. Simulates ICL crystallization.

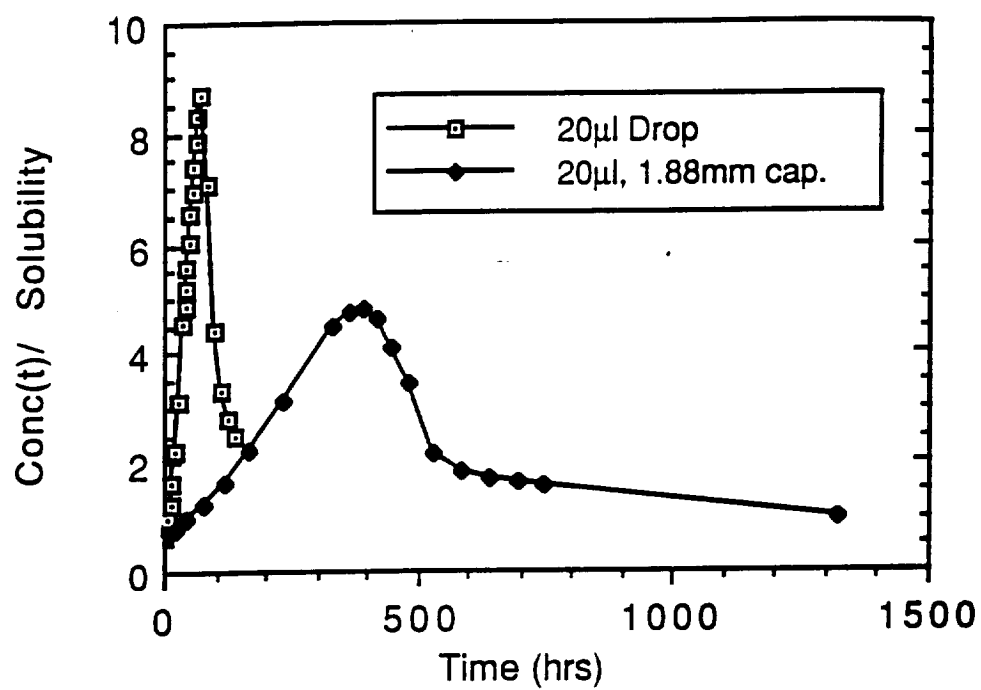


Fig. 6. Supersaturation vs. time for lysozyme comparing 20µl drop with 20µl in 1.88mm capillary. 10 crystals are nucleated at  $c/s = 4$  and allowed to grow.

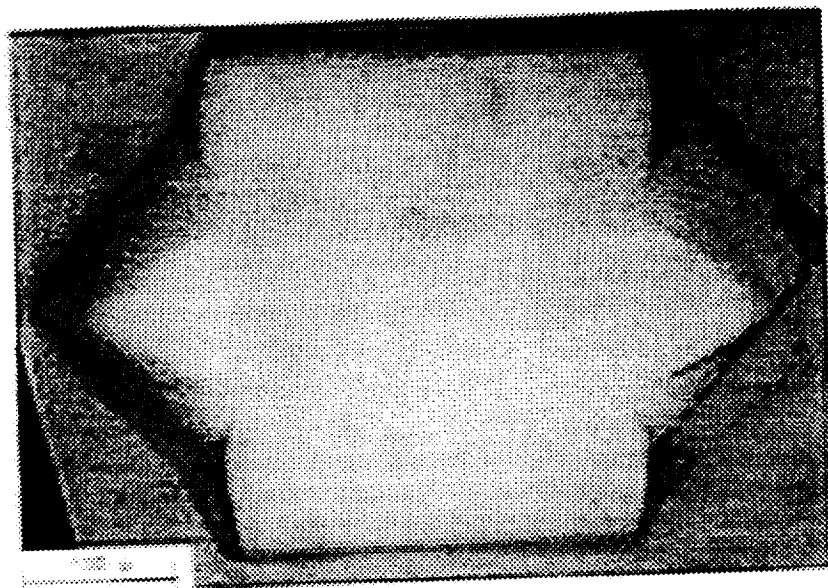


Fig. 7. ICL crystal grown from 30 $\mu$ l drop (10mg/ml) in  $\mu$ g.

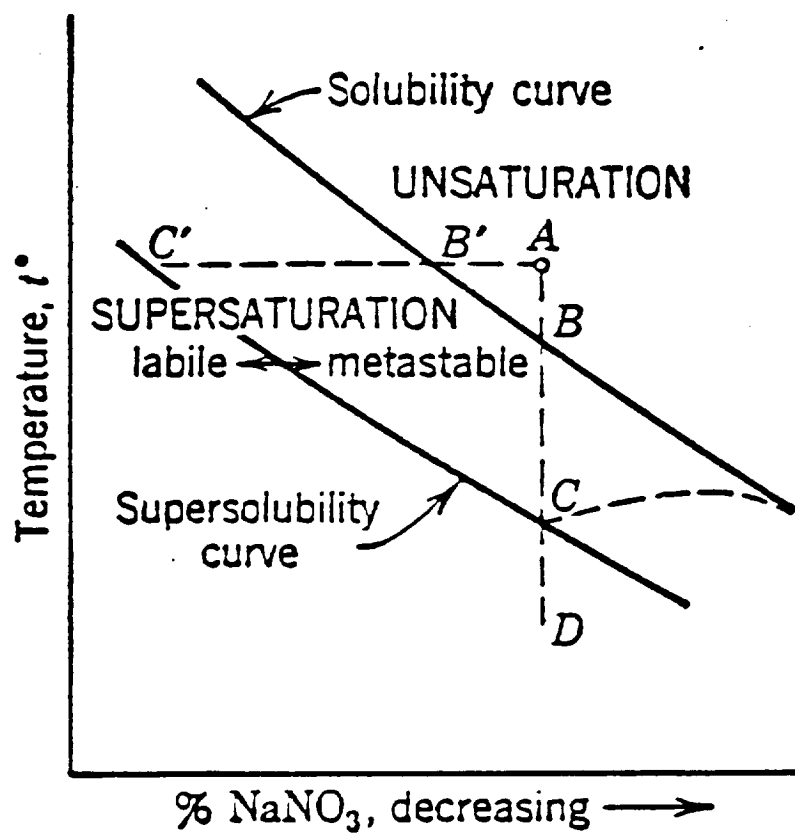


Fig. 8. Schematic diagram of solubility for a substance whose solubility increases with temperature.

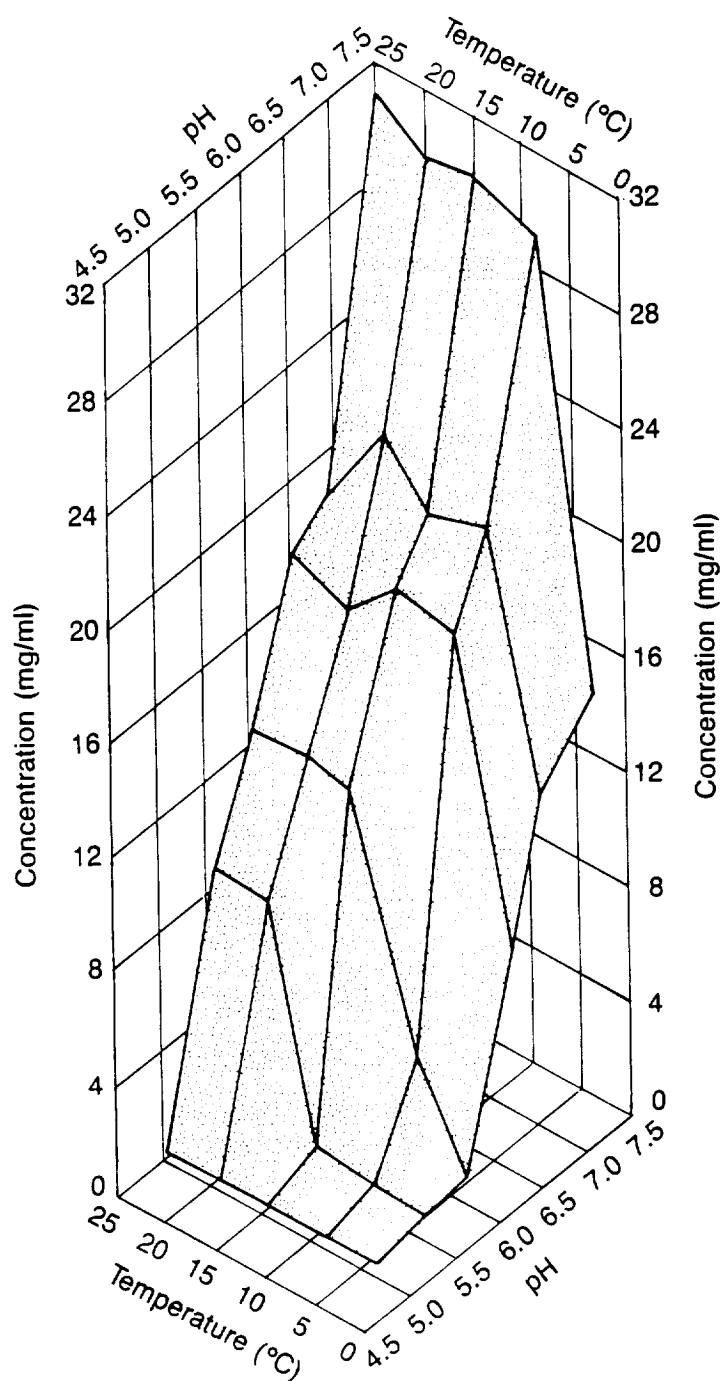


Fig. 9. Solubility diagram for canavalin showing dependence on temperature and pH.

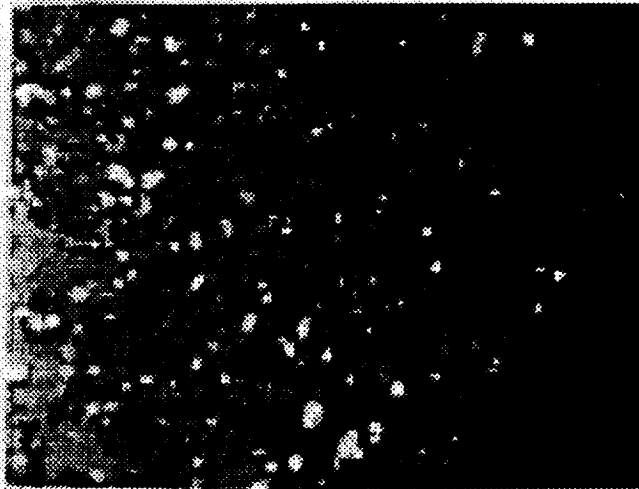


Fig. 10. Comparison of spontaneously nucleated (top) and temperature nucleated lysozyme crystals. Index spacing is 100 $\mu$ .

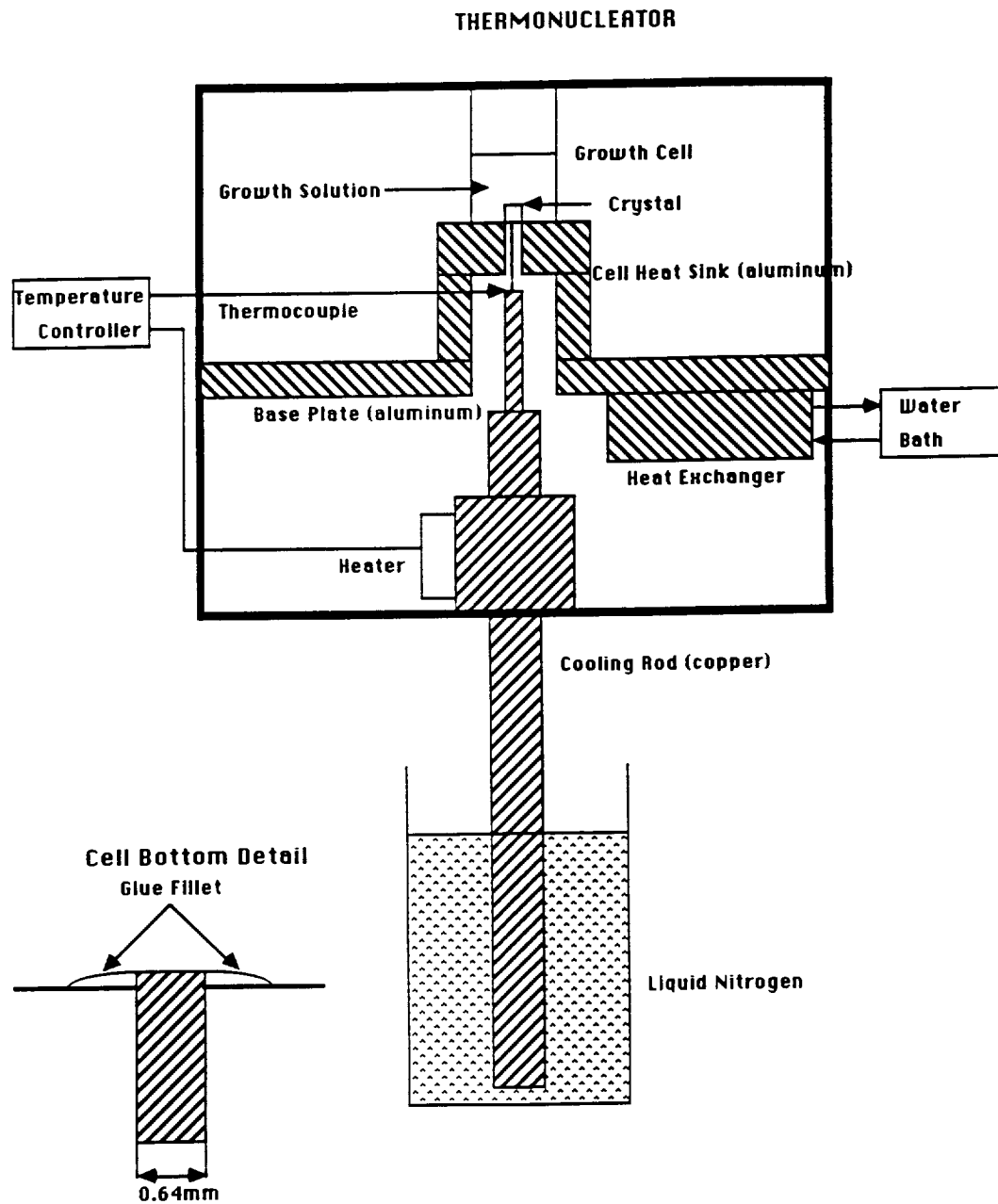


Fig. 11. Schematic of ThermoNucleator showing growth cell, cold spot, cold spot temperature control and ambient temperature control by heat exchanger.



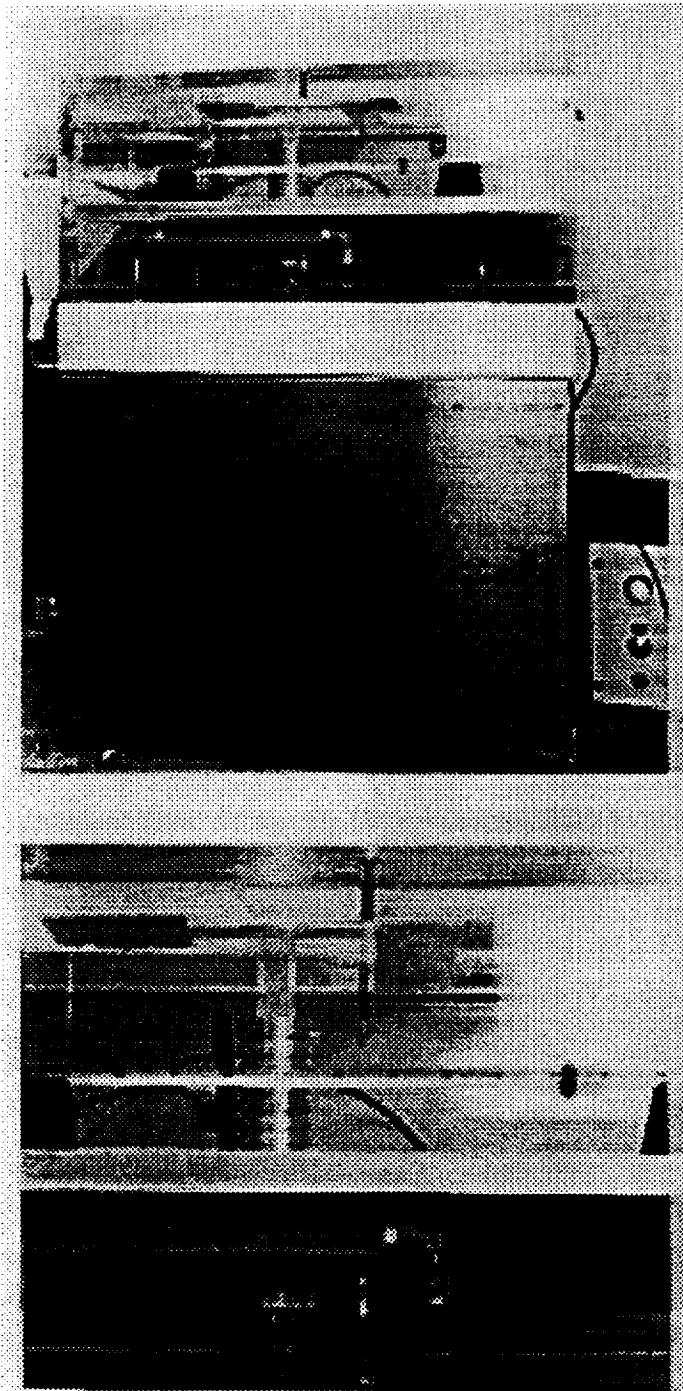


Fig. 12. Thermonucleator apparatus showing; Top: Growth cell and cell heat sink (above base plate), and heat exchanger and cold spot control (below base plate) [19.5in (h) 15 in (w)]. Bottom: Close-up of growth cell, cell heat sink control thermocouple, heat exchanger and cold spot heater.

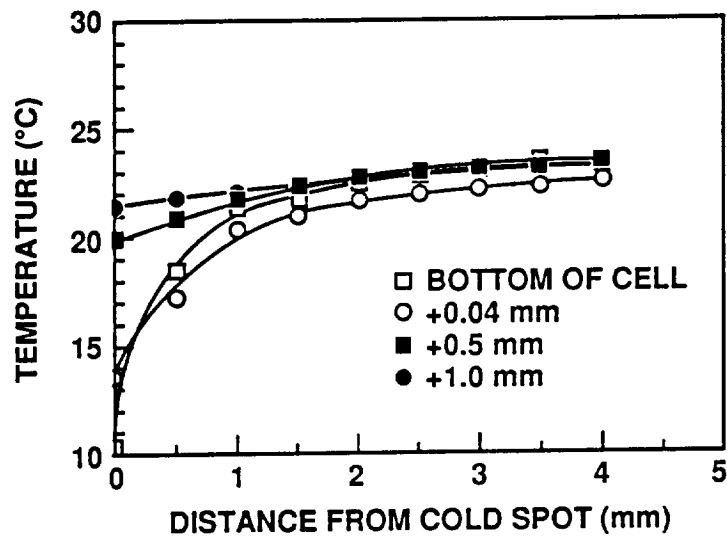


Fig. 13. Temperature gradients measured at various distances from the bottom of the growth cell in the Thermonucleator with a 25°C ambient and a 15°C cold spot.

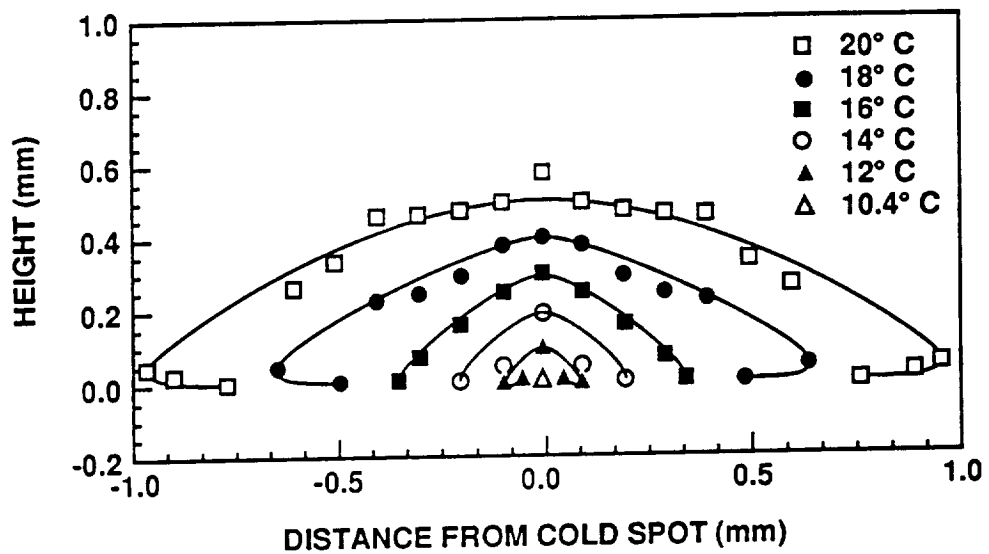


Fig. 14. Isotherms developed in growth cell of the Thermonucleator with a 25°C ambient and a 15°C cold spot.

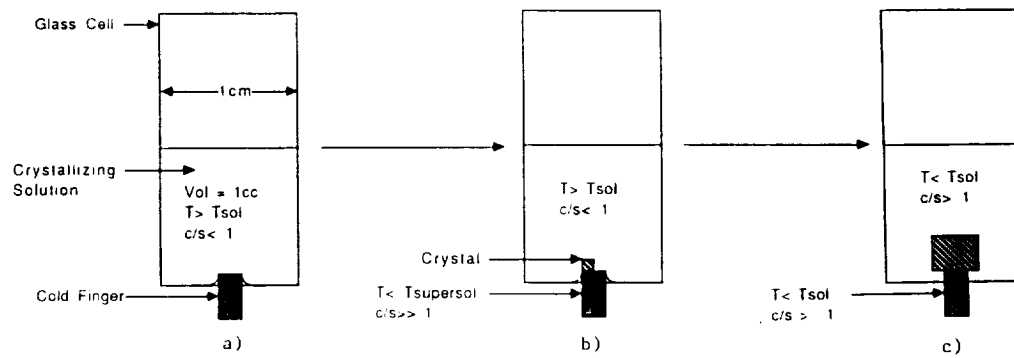


Fig. 15. Controlled nucleation using temperature control method (thermonucleation).

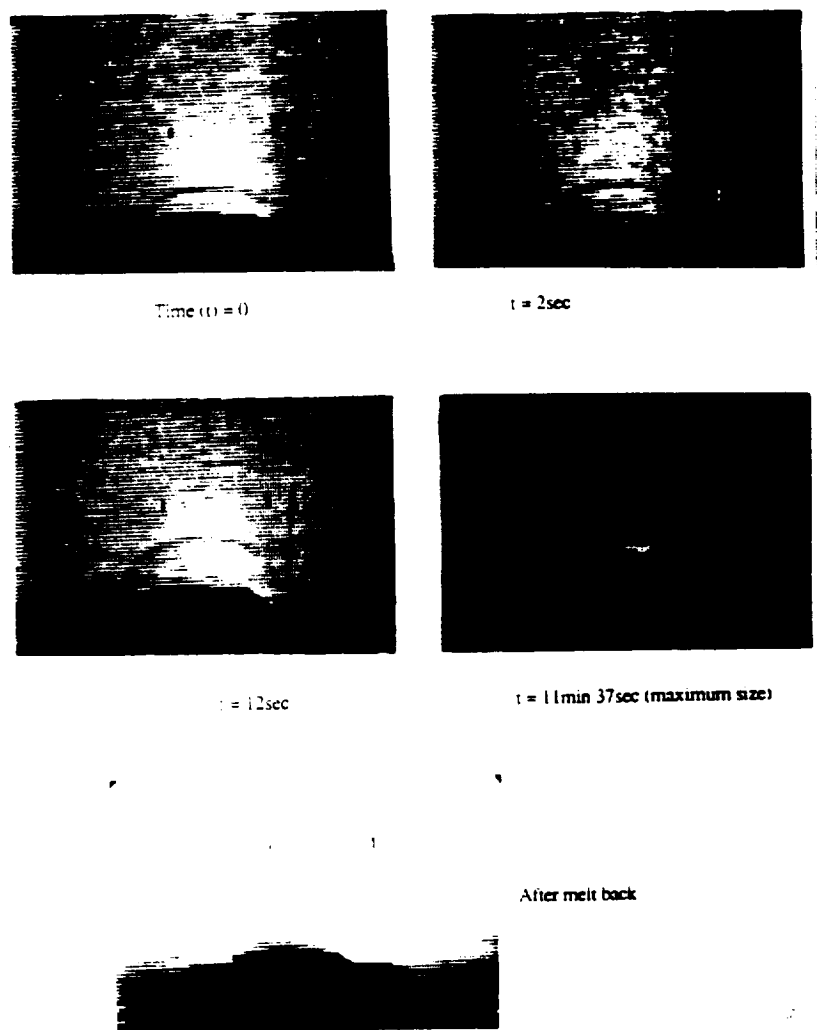


Fig. 16. Sequence of photographs showing the nucleation and growth of an ice crystal in the Thermonucleator.

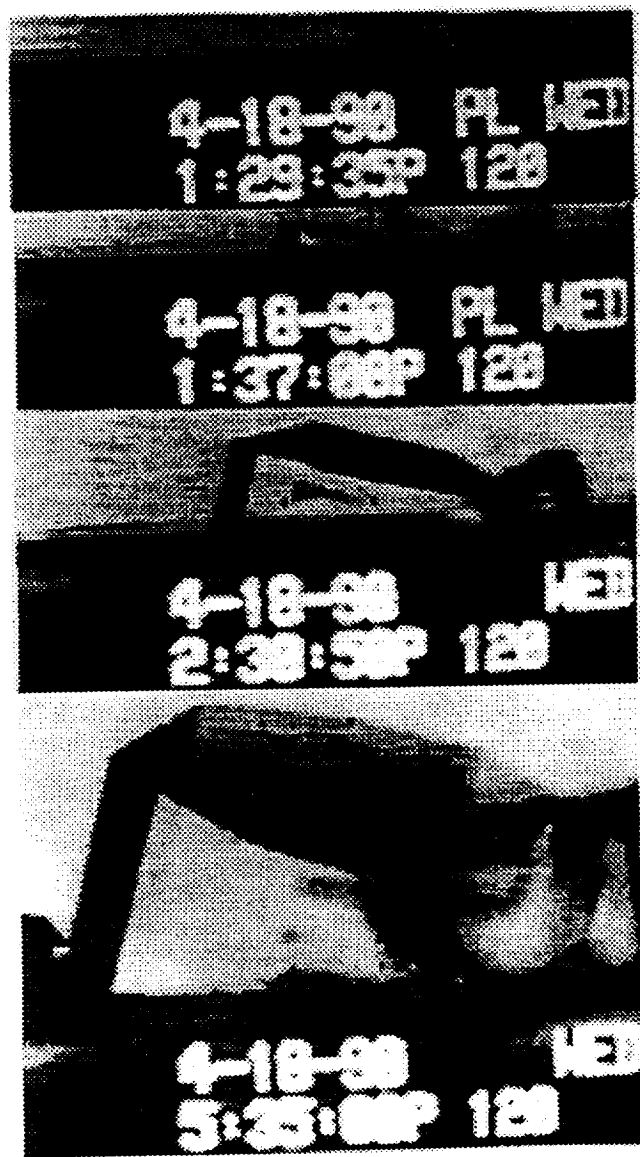


Fig. 17. Sequence of photographs showing the nucleation and growth of Rochelle salt in the Thernonucleator. Conditions: Top:  $T_e=24^{\circ}\text{C}$ ,  $T_s=16^{\circ}\text{C}$ ;  $T_e=24^{\circ}\text{C}$ ,  $T_s=16^{\circ}\text{C}$ ;  $T_e=22^{\circ}\text{C}$ ,  $T_s=T_e$  and Bottom:  $T_e=20^{\circ}\text{C}$ ,  $T_s=T_e$ .

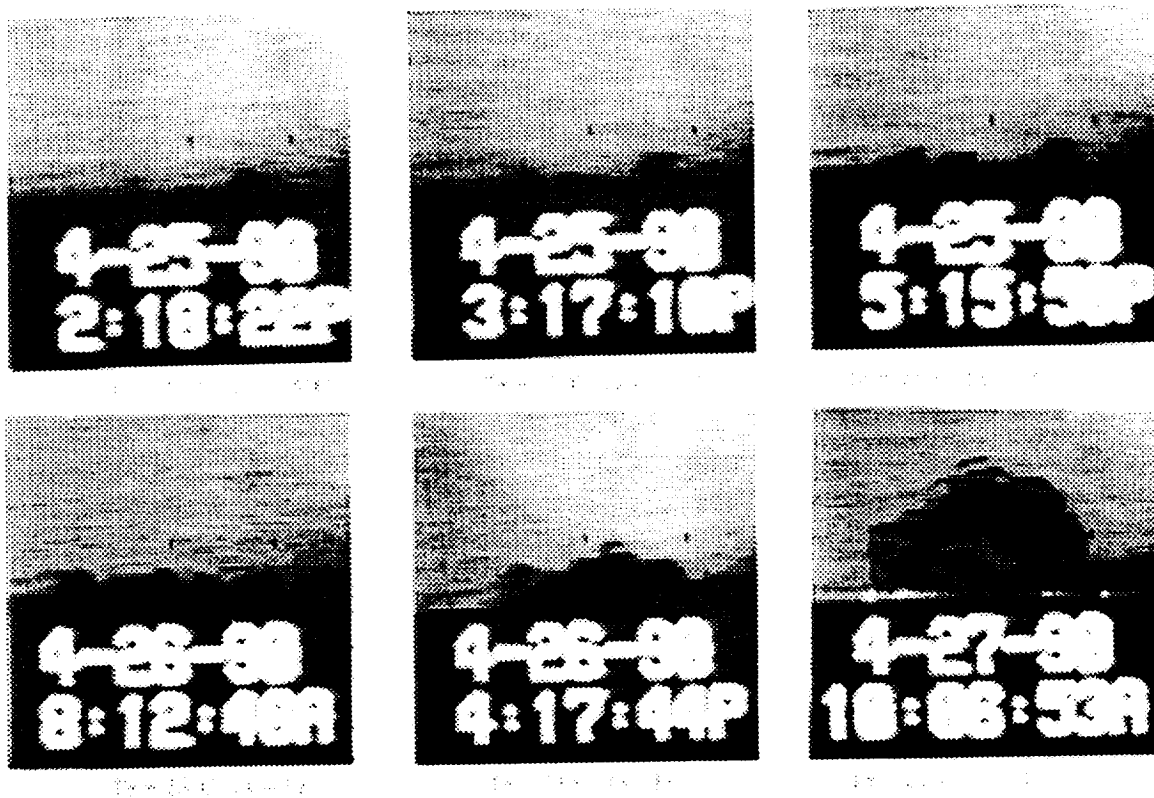


Fig. 18. Sequence of photographs showing the nucleation and growth of lysozyme in the Thermanucleator. Conditions: Top row, left:  $T_e=25^\circ\text{C}$ ,  $T_s=15^\circ\text{C}$ ;  $T_e=25^\circ\text{C}$ ,  $T_s=15^\circ\text{C}$ ;  $T_e=25^\circ\text{C}$ ,  $T_s=T_e$  and Bottom row, left:  $T_e=25^\circ\text{C}$ ,  $T_s=T_e$ ;  $T_e=23^\circ\text{C}$ ,  $T_s=T_e$ ;  $T_e=21^\circ\text{C}$ ,  $T_s=T_e$ .



Date	7-24	7-24	7-25	7-25	7-25	7-26	7-29	8-1	8-5
Time	1002	1309	0804	1217	1435	1639	1433	1622	0757
Elapsed Time (hrs)	0	3.12	20.02	24.24	26.54	52.31	119.21	193.03	280.61
Spot Temperature (°C) (c/s)	28 (.53)	12 (4.02)	22 (1.15)	28 (.53)	20 (1.50)	20 (1.50)	18 (1.98)	18 (1.98)	16 (2.57)
Ambient Temperature (°C) (c/s)	28 (.53)	22 (1.15)	20 (1.50)	26 (.66)	21 (1.31)	20 (1.50)	20 (1.50)	20 (1.50)	18 (1.98)
Size (μ)					147	191	224	269	269

Fig. 19. Photographs showing the results of the improved growth procedure for the growth of lysozyme.



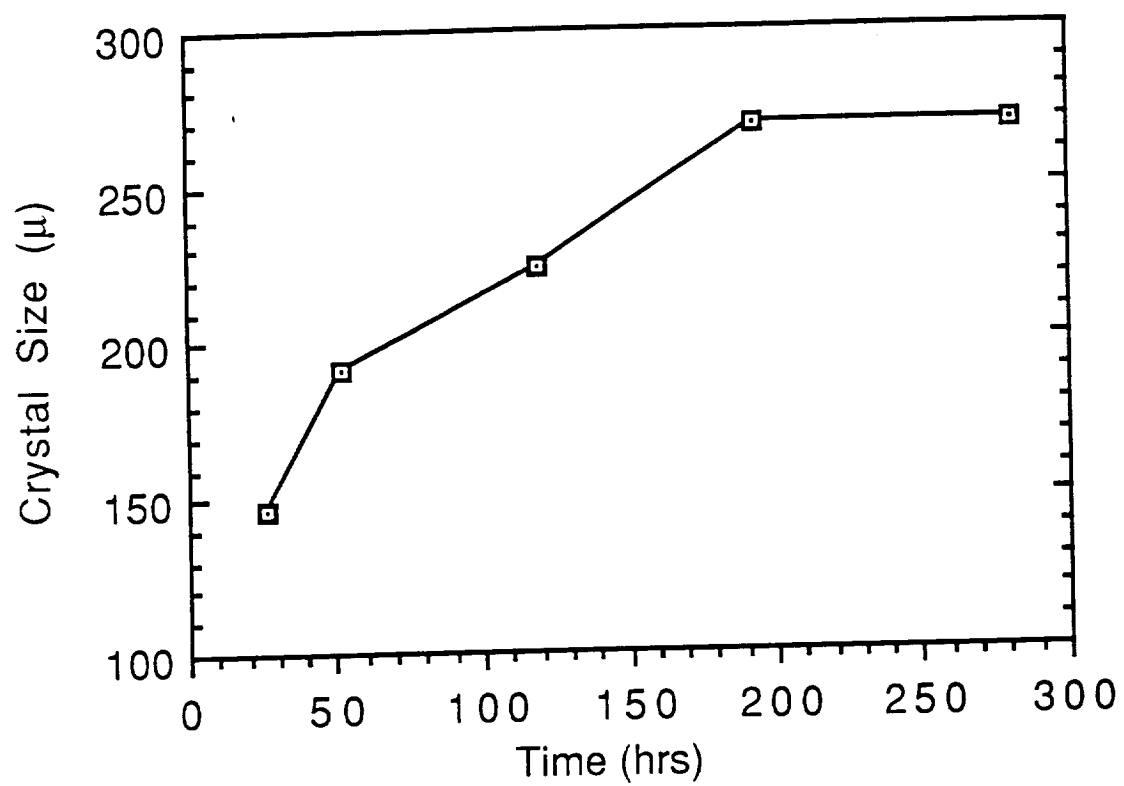


Fig. 20. Crystal size vs. time for lysozyme crystal grown in latest experiment.

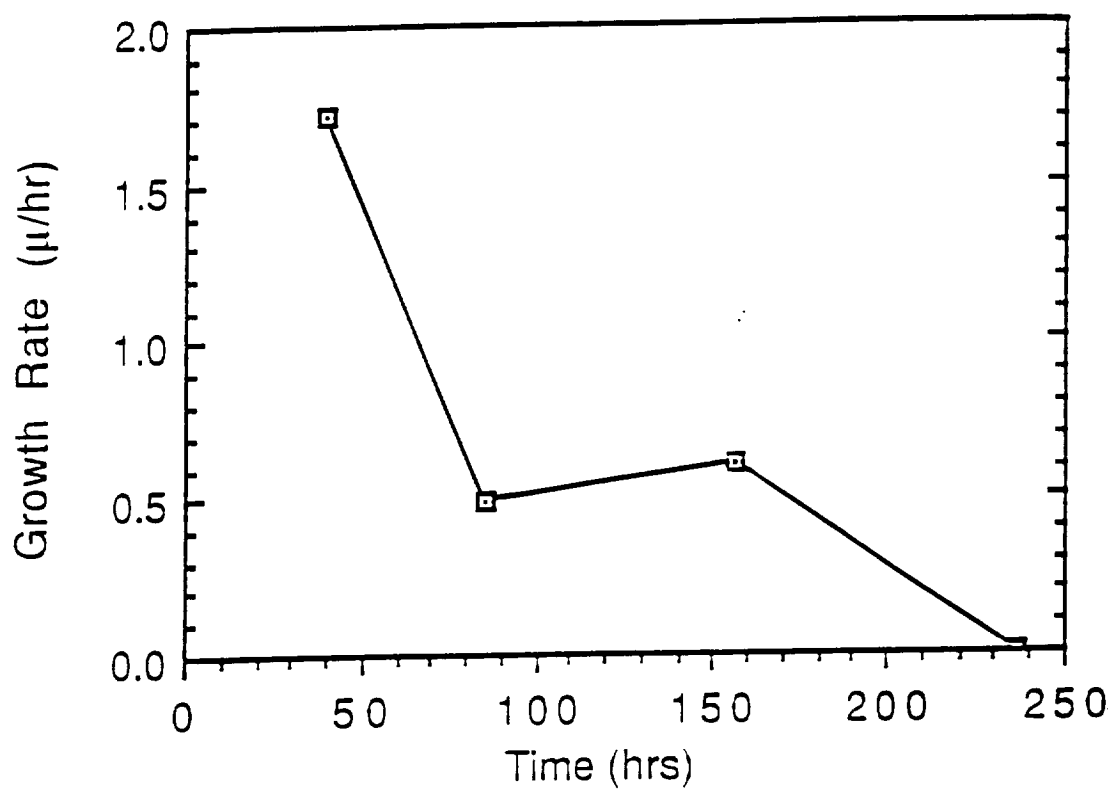


Fig. 21. Growth rate vs. time for the lysozyme crystal in Fig. 19.

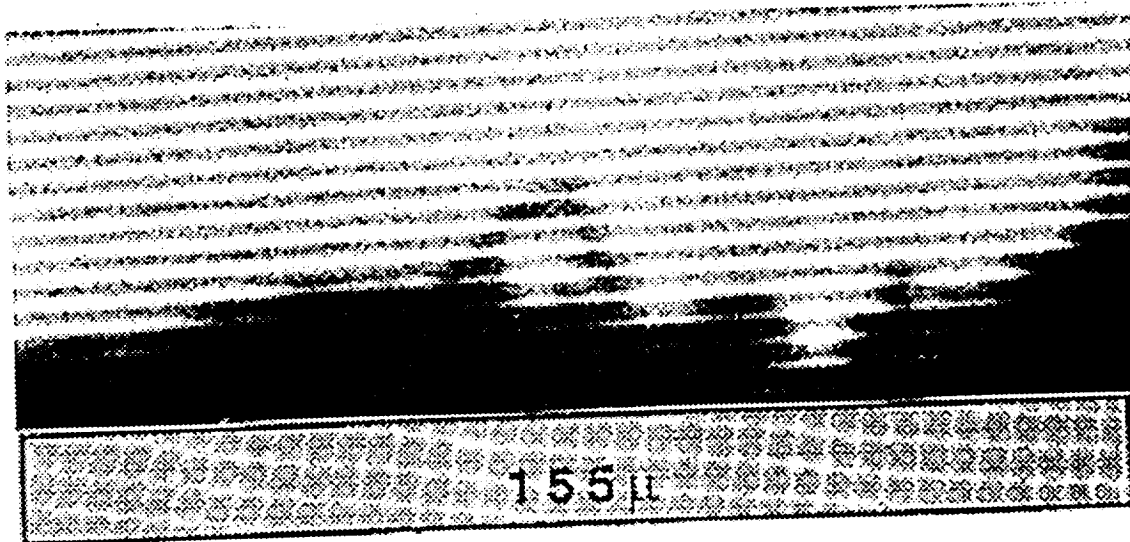


Fig. 22. Horse serum albumin crystal nucleated in the Thermonucleator. Textured area shows location of a section of the temperature controlled probe. Apparent rough surface is due to the presence of several smaller nuclei. Photographed from a TV monitor.

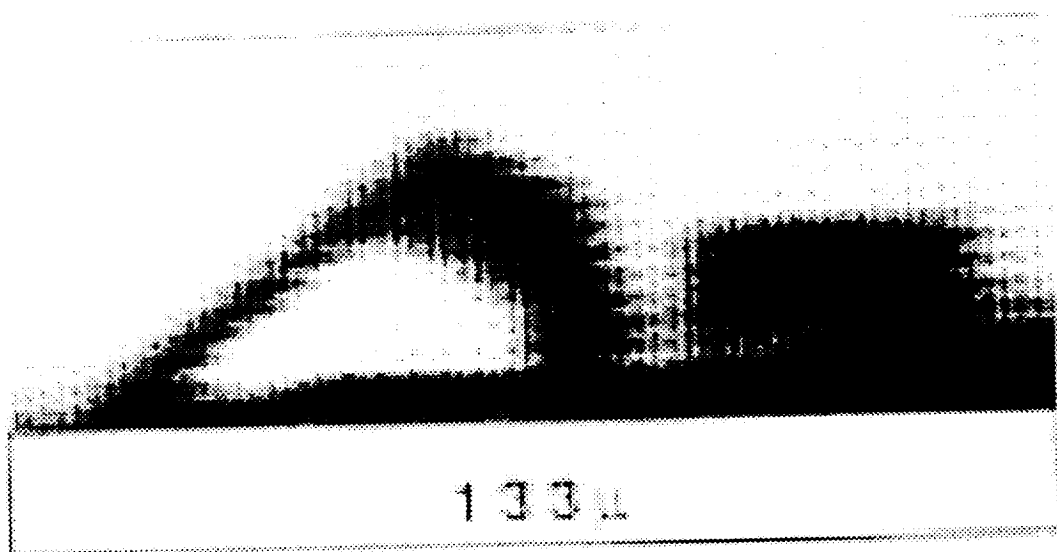
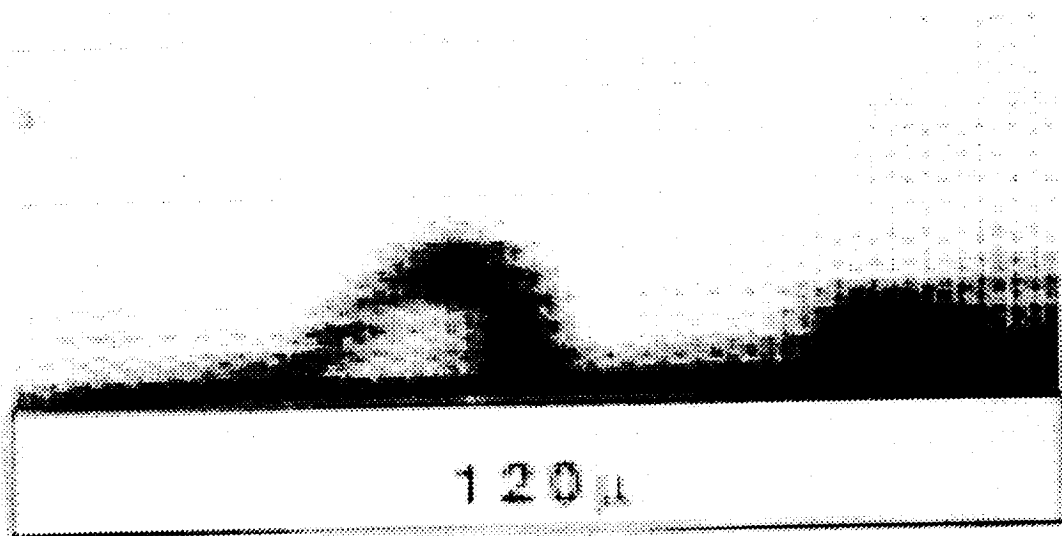


Fig. 23.  $\alpha$ -chymotrypsinogen A crystals nucleated in the Thermonucleator; a) shortly after appearance of the crystals, b) after one week of growth. Textured area shows location of a section of the temperature controlled probe. Photographed from a TV monitor.

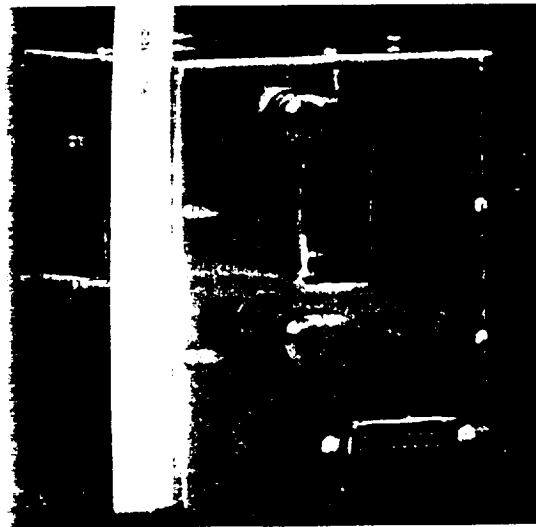
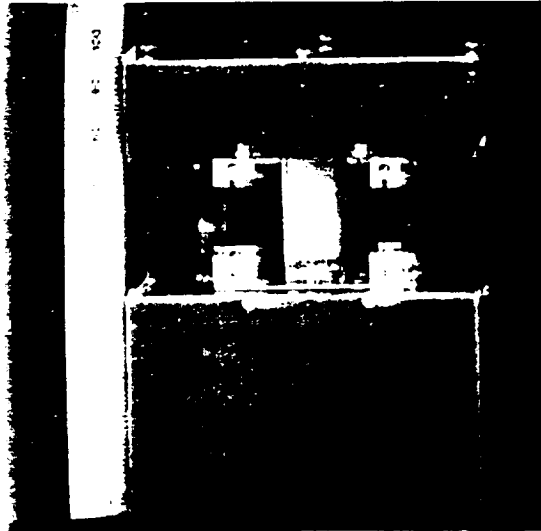


Fig. 24. Latest design of the Thermonucleator showing: top) front view and bottom) rear view with coolant and electrical connections, and port for illumination. Scale is in mm.

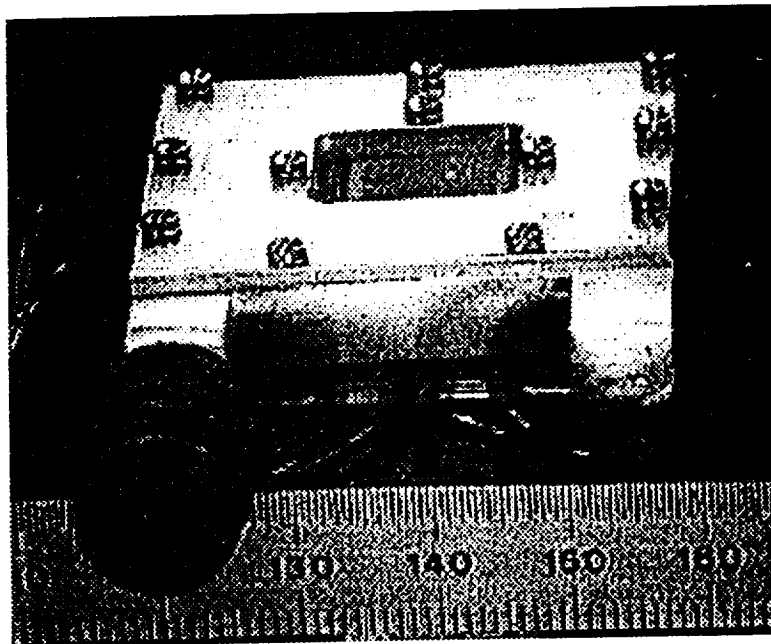


Fig. 25. Thermoelectric cooling module for controlling ambient in the Thermonucleator.

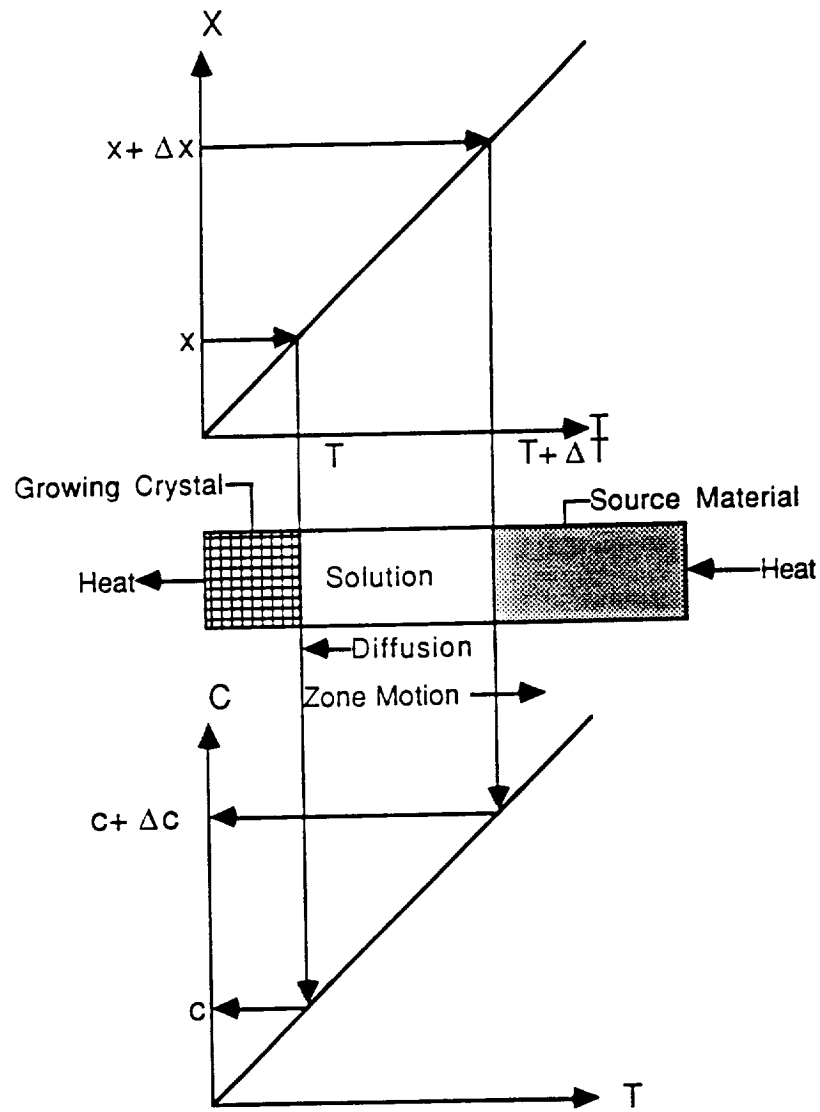
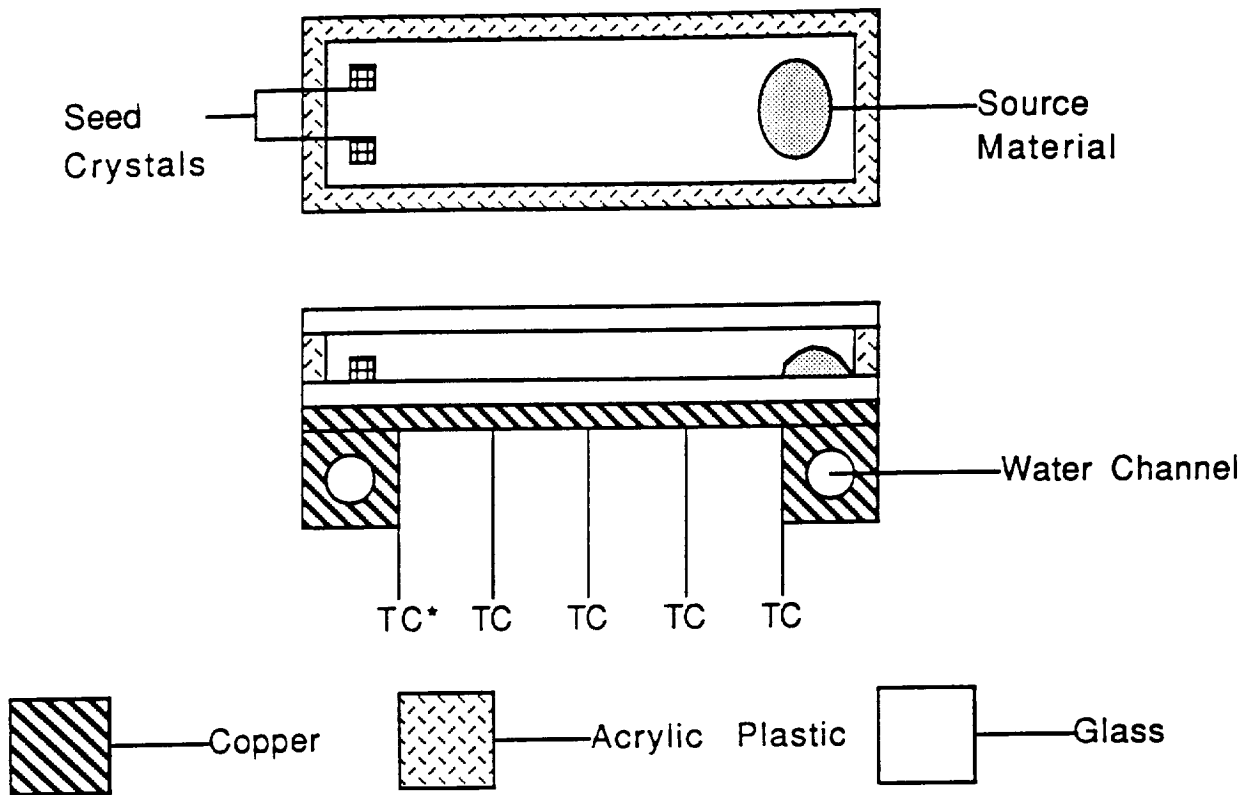


Fig. 26. Relationship between temperature gradient and solubility for a theoretical material exhibiting normal solubility.

# $\Delta T$ GROWTH CELL



\* Thermocouple

Fig. 27. Temperature gradient cell. Thermocouples are indicated by TC.



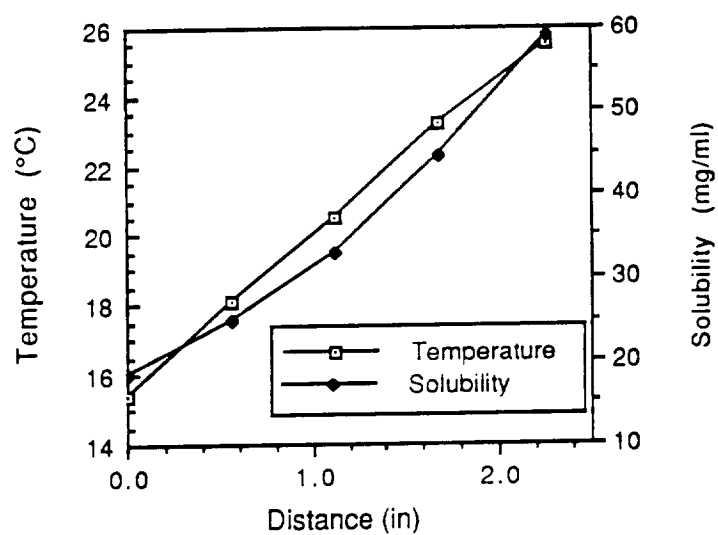


Fig. 28. Temperature and solubility gradients developed in temperature gradient cell.

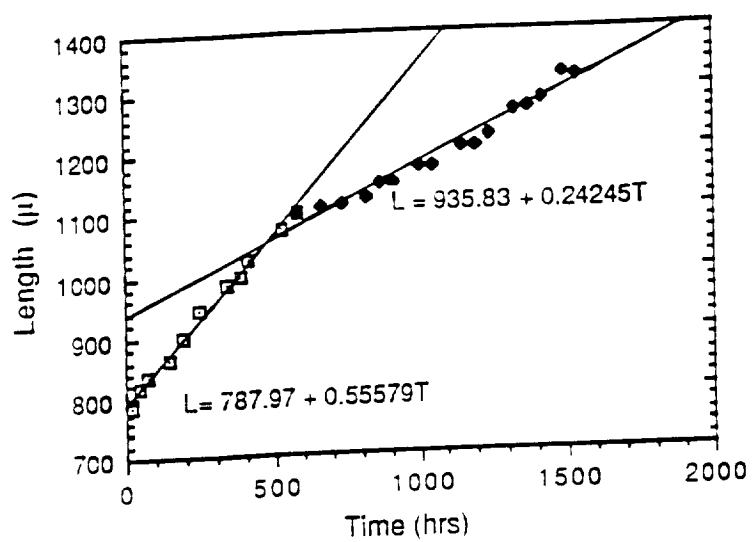


Fig. 29. Size vs. time for a lysozyme crystal grown under the conditions of Fig. 28.

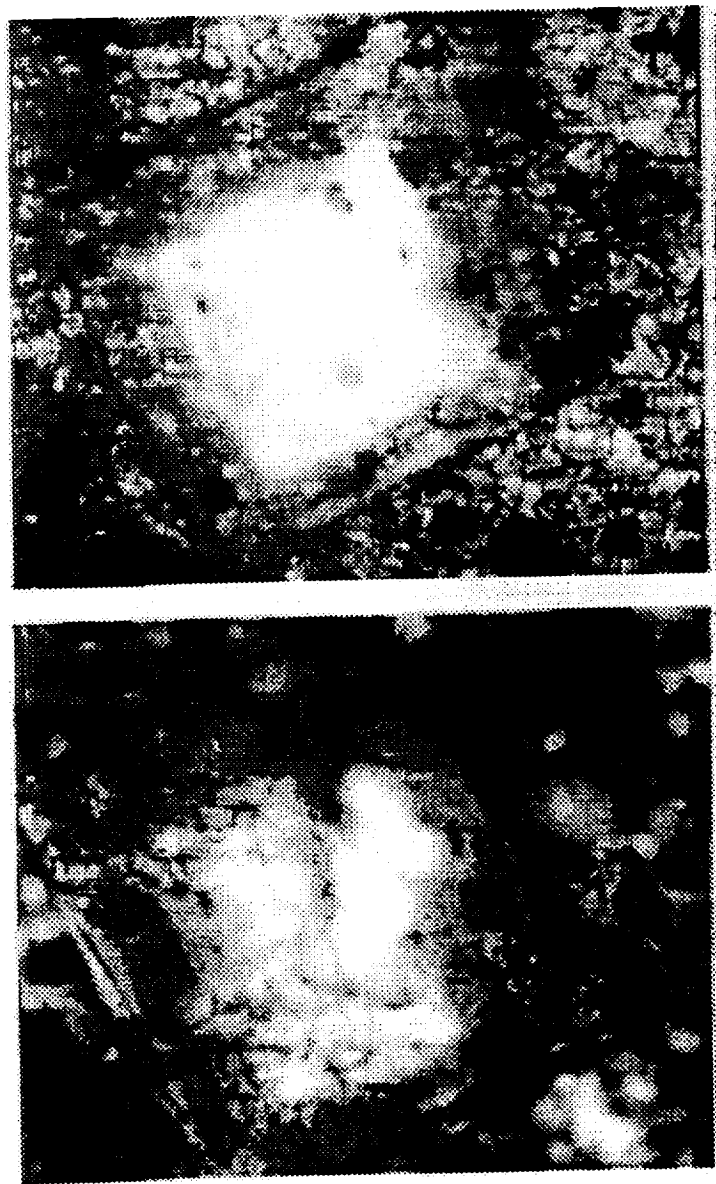


Fig. 30. Lysozyme crystal grown under conditions of Fig. 28 photographed in transmitted light with crossed polarizers.  
Top) Secondary nucleation evident. Light area was the seed.  
Bottom) Surface morphology developed during growth. Crystal size was  $1320\mu$ .

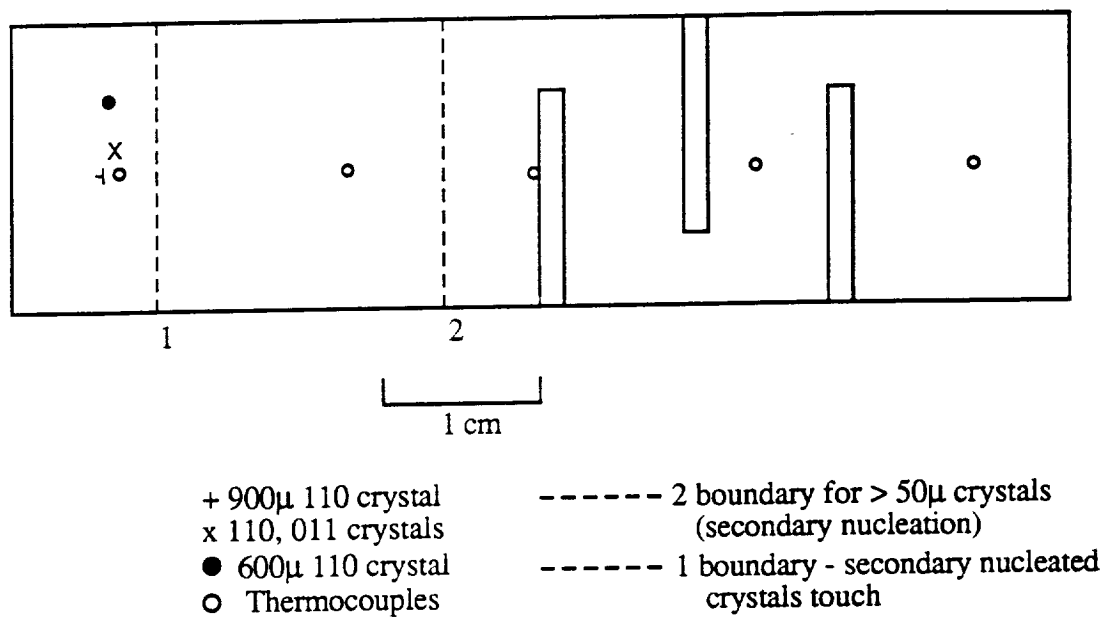
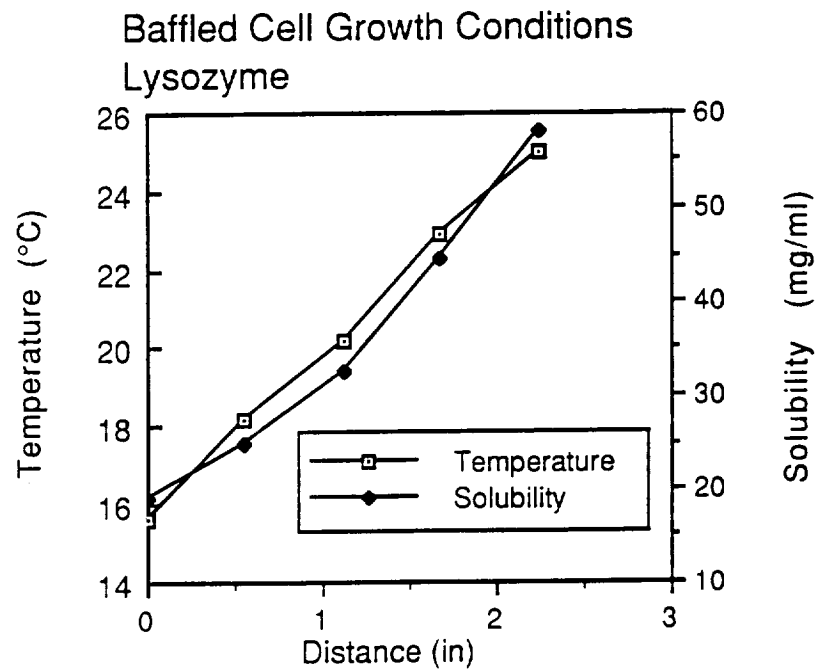


Fig. 31. Baffled cell design to eliminate drift of source material. Location of seeds, secondary nucleation and thermocouple are indicated.



Expected Growth Rate -  $0.44\mu/\text{hr}$  (Pusey and Naumann)

Fig. 32. Temperature and solubility gradients developed in baffled cell.

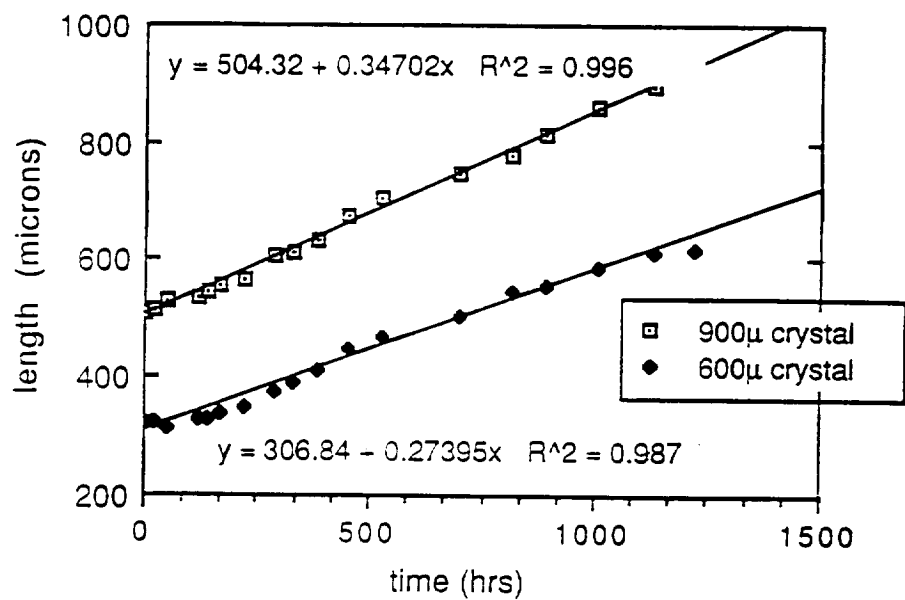


Fig. 33. Size vs. time for lysozyme crystals grown under the conditions of Fig. 32.



Fig. 34. Lysozyme crystals grown under the conditions of Fig. 32.  
Top) 922 $\mu$   
Bottom) 617 $\mu$ .

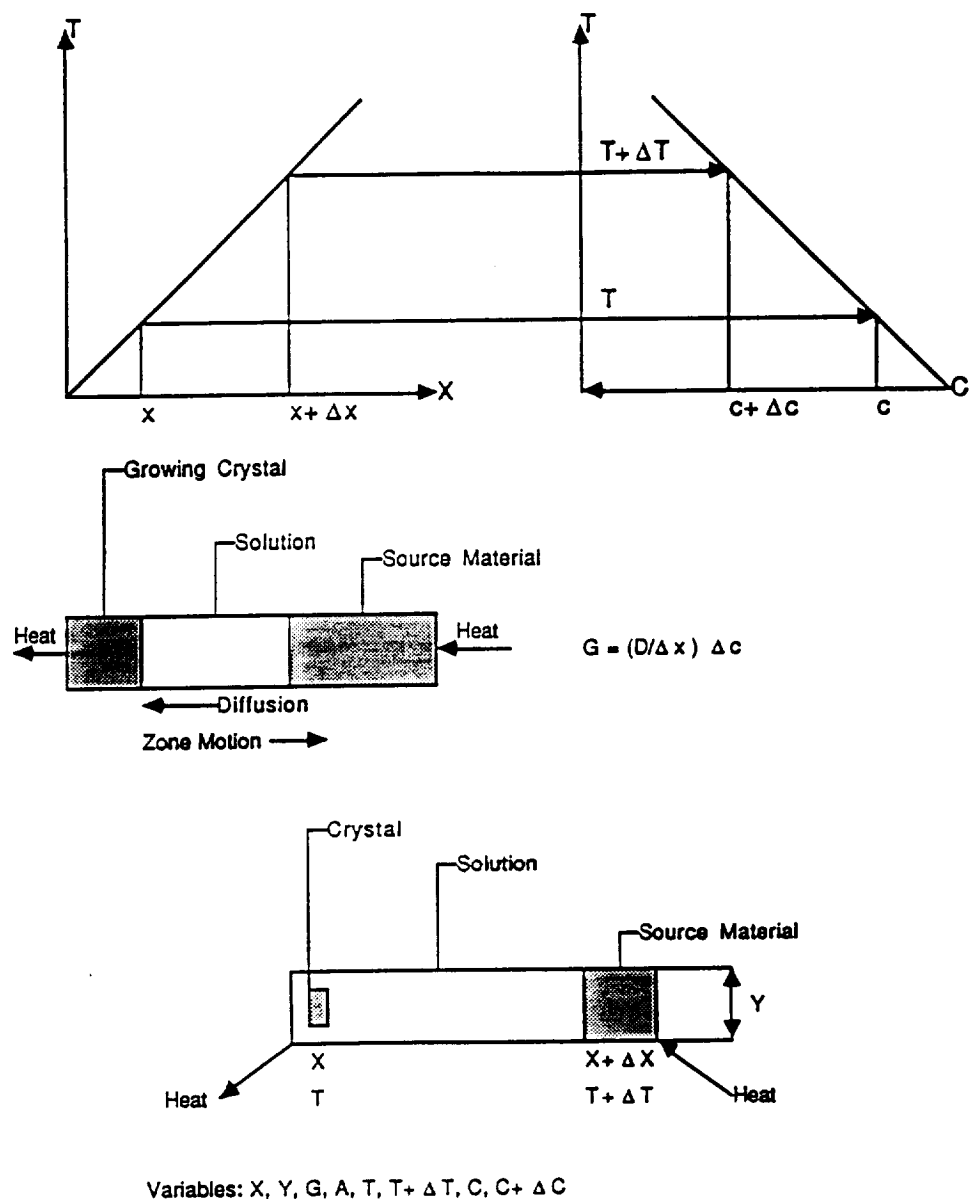


Fig. 35. Parameters of temperature gradient growth technique.



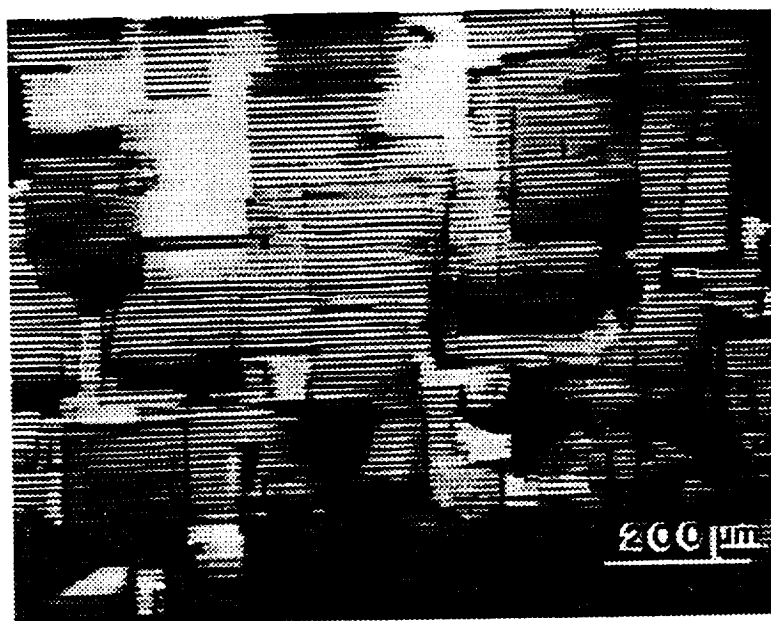


Fig. 36. Catalase crystals deposited at relatively low supersaturations.

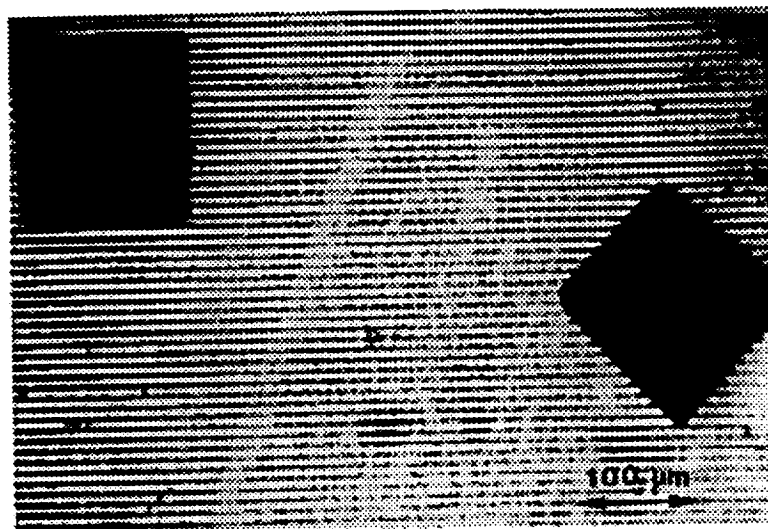


Fig. 37. Diagonal of orientation.



Fig. 38. Backside of a catalase crystals removed from the substrate. Note parallel striation (with a period equal to that of striated micro-relief) as a result of the crystal growing into the substrate after a long period of time (about 3 days) in a supersaturated solution.

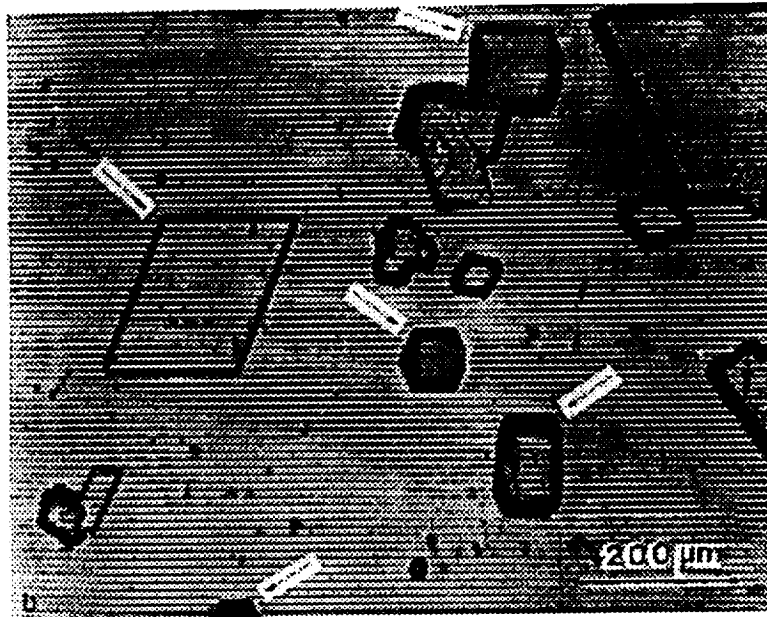


Fig. 39. Crystals of canavalin oriented parallel to striations (as indicated by arrows) together with crystals having different orientations.

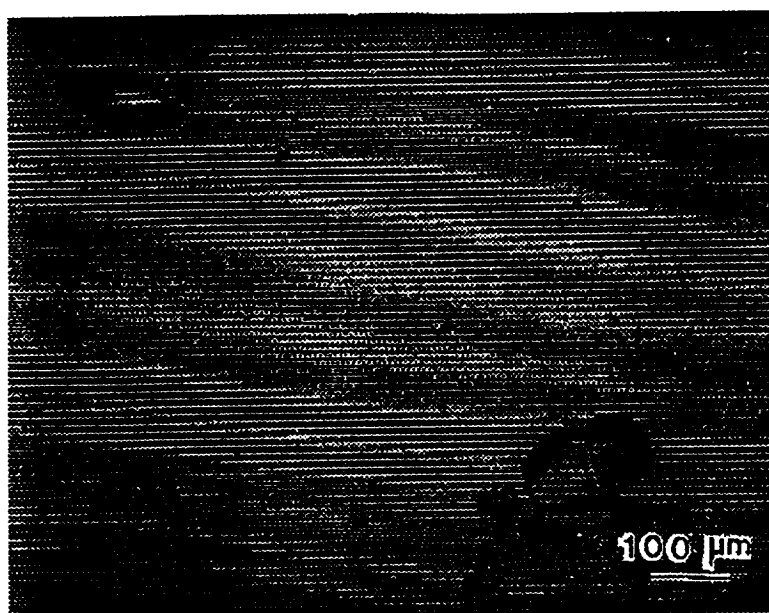


Fig. 40. Lysozyme crystals deposited in orientation positions with respect to striated micro-relief.

